General Disclaimer

One or more of the Following Statements may affect this Document

- This document has been reproduced from the best copy furnished by the organizational source. It is being released in the interest of making available as much information as possible.

- This document may contain data, which exceeds the sheet parameters. It was furnished in this condition by the organizational source and is the best copy available.

- This document may contain tone-on-tone or color graphs, charts and/or pictures, which have been reproduced in black and white.

- This document is paginated as submitted by the original source.

- Portions of this document are not fully legible due to the historical nature of some of the material. However, it is the best reproduction available from the original submission.

Produced by the NASA Center for Aerospace Information (CASI)

IITRI

N70-15581
(ACCESSION NUMBER)
73
(PAGES)
CR-102413
(NASA CR OR TMX OR AD NUMBER)
1
(THRU)
(CODE)
13
(CATEGORY)
FACILITY FORM 602

APR 1969
RECEIVED
NASA STI FACILITY
INPUT BRANCH

FINAL REPORT

J6096

ATMOSPHERIC DESIGN CONCEPTS FOR CROSS-BEAM EXPERIMENTS

National Aeronautics & Space Administration

Huntsville, Alabama

NAS8 - 20107

FINAL REPORT

J6096

ATMOSPHERIC DESIGN CONCEPTS FOR CROSS-BEAM EXPERIMENTS

Prepared by

R. D. Sears

of

IIT Research Institute
Chicago, Illinois 60616

for

National Aeronautics & Space Administration
George C. Marshall Space Flight Center
Huntsville, Alabama

April 1969

IIT RESEARCH INSTITUTE

FOREWORD

This is the Final Report on Contract NAS8-20107 Mod. 3 entitled,"Atmospheric Design Concepts for Cross-Beam Experiments". This research was related to evaluating the feasibility of utilization of the cross beam remote sensing technique for atmospheric research problems.

In addition to the author, principal contributors to this research were R. W. Deuel, J. W. Helbron and G. L. N. Rao. Other contributors were M. W. P. Cann, W. O. Davies, G. Owen and G. Johnson.

Respectfully submitted,
IIT RESEARCH INSTITUTE

Robert D. Sears
Senior Scientist,
Group Leader
Plasma Physics

APPROVED BY:

C. A. Stone, Director
Physics Division

PRECEDING PAGE BLANK NOT FILMED

TABLE OF CONTENTS

		Page
I.	INTRODUCTION	1
II.	ANALYTICAL STUDY OF FLUCTUATIONS SOURCES IN THE ATMOSPHERE	2
	A. Lower Atmosphere Sources of Probing Signals	2
	B. Nonthermal Radiation from the Upper Atmosphere	27
	C. Atmospheric Fluctuations at High Altitudes	33
	D. Determination of Mean Values of Number Density from Volume Emission Rate Fluctuations	39
	E. Oxygen Allotrope Photochemistry	44
III.	SUMMARY AND CONCLUSIONS	61
	REFERENCES	62

FIGURE CAPTIONS

Figure		Page
1	Aerosol Number Density as a Function of Altitude	4
2	Sky Spectral Luminance versus Altitude H	5
3	Relationship between the Zenith Angles and the Scattering Angle on the Celestial Sphere	6
4	Effect of Surface Reflectance on Sky Spectral Luminance	7
5	Effect of Solar Zenith Angle on Sky Spectral Luminance	8
6	Effect of Observational Zenith Angle θ_o on Sky Spectral Luminance	9
7	Effect of Wavelength on Zenith Luminance vs. Solar Zenith Angle	10
8	Effect of Projected Observation Zenith Angle on Spectral Luminance vs. Projected Azimuth: Solar Zenith Angle θ_o = 37 degrees λ = 0.55 μ	11
9	Effect of Observational Zenith Angle θ on Spectral Luminance vs. Projected Azimuth Solar Zenith Angle θ_o = 66 degrees λ = 0.55 μ	12
10	Effect of Observational Zenith Angle θ on Spectral Luminance vs. Projected Azimuth λ = 0.55 μ	13
11	Zenith Sky Spectral Luminance	17
12	Relative Contribution of Aerosol Scatter and Ozone Extinction of Total Extinction Coefficients	18
13	Total Extinction Coefficients as a Function of Altitude and Wavelength	19
14	Emission Spectrum of Atmospheric Radiation Background for Two Altitudes	21

FIGURE CAPTIONS - Cont'd

Figure		Page
15	Infrared Sky Spectrum Observed on a Clear Night. The Upper Curve Gives a Solar Spectrum for Comparison	22
16	Altitude at which Solar Ultraviolet Radiation is Reduced to a Value of e^{-1} of its Original Intensity	25
17	Night Sky Emission Spectrum 0.3 to 1.0 Micron	28
18	Ratio of Line Intensity to Background Intensity vs. Zenith Spectral Luminance for Parametric Values of Filter Passbands	31
19	OI Energy Level Diagram	45
20	O_2 Energy Level Diagram	46
21	$O(^1D)$ Production Rates vs. Altitude	49
22	$O(^1D)$ Loss Rate - sec^{-1}	50
23	Atomic Oxygen Density Profile (CIRA 1965) and Chapman Reaction, $O(^1S)$ Production vs. Altitude	51
24	De-Activation Rate of Excited Oxygen Atoms (^1S) vs. Altitude by Reaction $O(^1S) + o(^3P)$ $2O(^1D)$	52
25	O_2 ($1\Sigma_g^+$) Formation Reaction	53
26	O_2 ($1\Delta_g$) Formation Rates vs. Altitude	54
27	Computed Volume Emission Rates vs. Altitude for O_2 Atmospheric Bands and OI, 5577 Å Radiation	55

I. INTRODUCTION

The goal of the subject research contract was to evaluate the feasibility of application of the cross beam remote sensing technique to problems in atmospheric physics. To accomplish this goal, a study was made of the sources of probing signals in the lower and upper atmosphere, the fluctuation properties of the atmosphere at high altitudes and the detailed theory required to relate the mean value properties of the atmosphere at high altitudes to the experimentally measurable cross beam variables (e.g. two beam fluctuation products, correlation functions, and fluctuation power spectra). To demonstrate the applicability of the cross beam method to upper atmospheric remote sensing, the specific case of the determination of the atomic oxygen density profile at high altitudes by cross beam measurements was worked out.

Emphasis was placed mainly upon atmospheric processes occurring at high altitudes because investigations of the feasibility of application of the cross beam method to the lower altitude regime were currently underway at Midwest Research Institute.[1] In addition, experimental investigations related to lower atmospheric wind and turbulence which utilized apparatus developed at IITRI under contract to MSFC were being conducted at IITRI[2] and CSU[3], in a cooperative program initiated by MSFC. The high altitude applications of the cross beam method discussed herein are based on concepts and theory developed for the laboratory applications to turbulent flows by Fisher et al,[4] to atmospheric applications concepts by Davies and Deuel,[5] and others.[6-10]

II. ANALYTICAL STUDY OF FLUCTUATIONS SOURCES IN THE ATMOSPHERE

In this section we examine the characteristics of probing signals which can be used with the cross beam remote sensing technique. The types of sources, the kinds of fluctuations which may modulate their received intensity, their altitude distribution, and the relationship of the signal characteristics to the source characteristics are all considered. The intensity fluctuation of a probing signal which passes through the atmospheric experimental volume, or is emitted therefrom, is the direct result of fluctuations of either the number density or the interaction coefficient of the atmospheric constituents with the probing signal. In this study we consider fluctuations of number density of an emitting species, and fluctuations in number density of an absorbing or scattering species. Previous work by Davies (Ref. 11) considers the case of thermal fluctuations wherein both partial pressure and temperature may vary.

Two general areas have been considered in the analytical study of fluctuation sources and probing signals: the sources of probing signal emission or modulation in the atmosphere as a function of wavelength and altitude, and their relationship to upper atmospheric turbulent structure and to the mean density profiles of minor species of aeronomical interest. In both cases, the mechanisms which cause the probing signal intensity fluctuations must be understood in order to relate the measurements to the atmospheric processes of interest.

A. Lower Atmosphere Sources of Probing Signals

The atmosphere may be treated both as a source of a probing signal and as a medium for modulation of an externally generated probing signal. Both of these effects may be described as a function of altitude in the atmosphere, as a function of wavelength, and as a function of the particular cross beam configuration to be

used, i.e., satellite, aircraft, or ground-based.

Scattering of sunlight by aerosols and molecular (Rayleigh) scattering processes is controlled primarily by the exponential atmospheric density distribution with altitude and by the aerosol distribution in the lower atmosphere. Because essentially 67 percent of the atmosphere is located in the lowest scale height ($\sim$6 km) and 90 percent in the lowest two scale heights ($\sim$12 km), it is clear that scattering processes as a source of probing signal are limited mainly to the troposphere. Figure 1 (Ref. 12) illustrates the observed altitude distribution of atmospheric density and a typical aerosol distribution. The falloff of sky spectral luminance as a function of altitude, which clearly follows the exponential behavior suggested in Figure 1, is illustrated in Figure 2 (Ref. 13).

The spectral luminance of the sky caused by multiple Rayleigh scattering is also a function of the observation angle with respect to the zenith and to the sun. Figure 3 illustrates the coordinates of the look angle, solar elevation, and zenith angle used in the family of graphs, Figures 4 through 10. Tabulations are available of relative spectral luminance at sea level in Reference 14. The data are tabulated for selected values of wavelength, λ; surface spectral reflectance, A; solar zenith angle, θ_o; observational zenith angle, θ; and projected observational azimuth, ϕ, referred to as the solar azimuth. Absolute sky spectral luminances were calculated from these relative values for selected examples by multiplying by the mean incident solar flux densities given in Table I[15] and by dividing by 2π. Figures 4 through 10 describe graphically the contents of the lengthy tables and indicate the relative effects of variation of the parameters.

Figure 4 shows that zenith spectral luminance increases by approximately a factor of 2 with increased surface reflectance (A) from 0 to 0.8 whereas the effect of wavelength change from

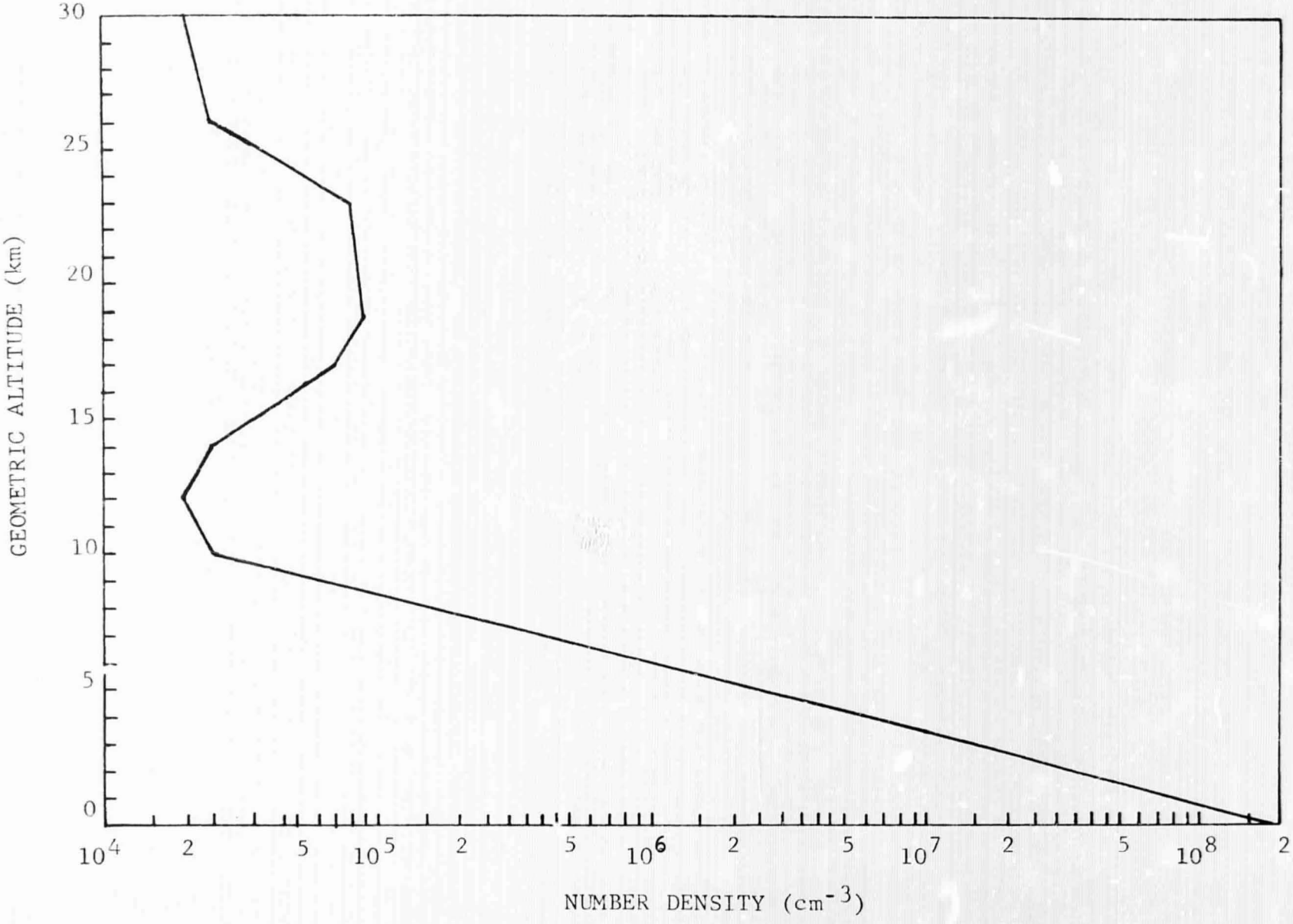


FIG. 1 Aerosol Number Density as a Function of Altitude

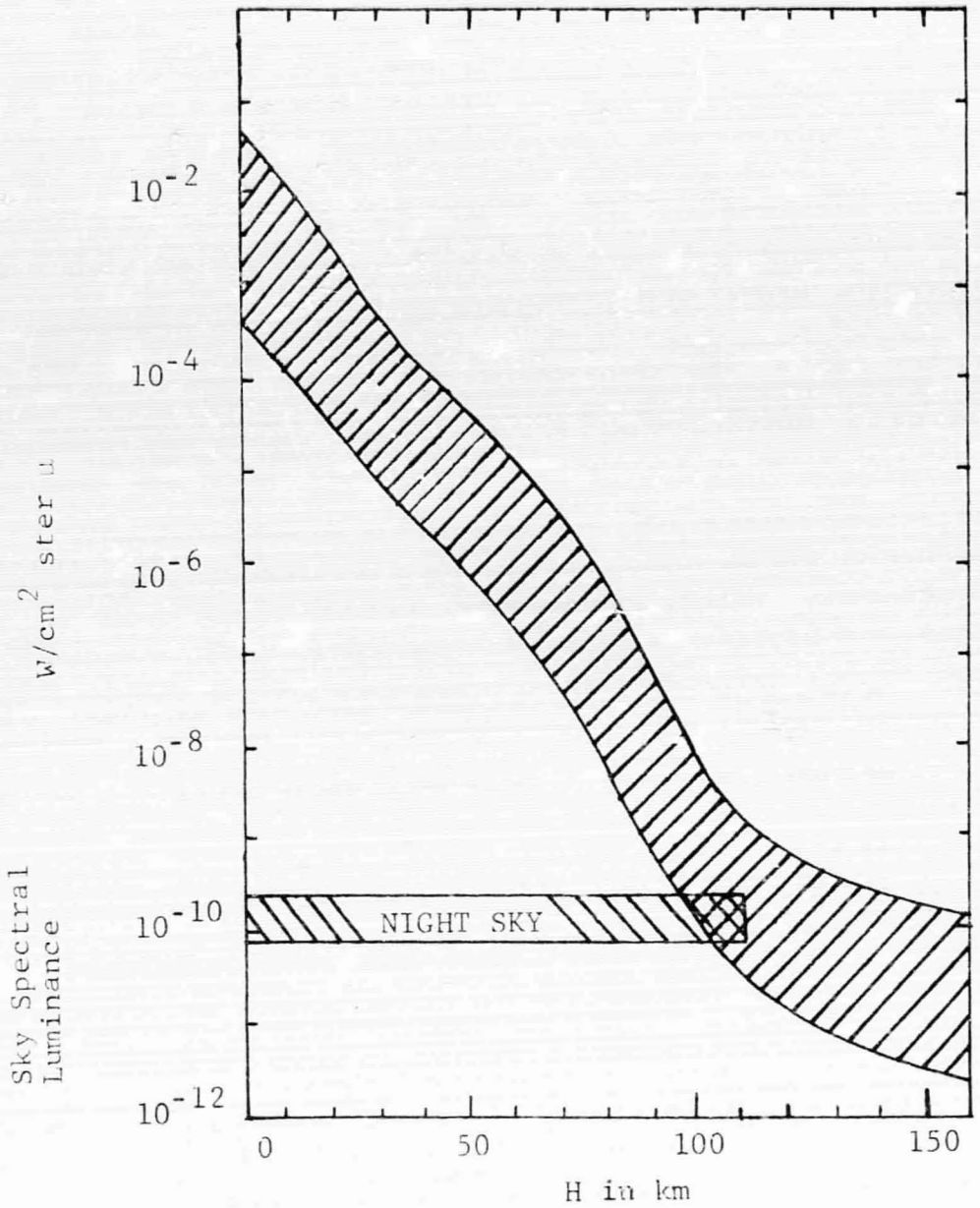


Fig. 2 Sky Spectral Luminance versus Altitude H

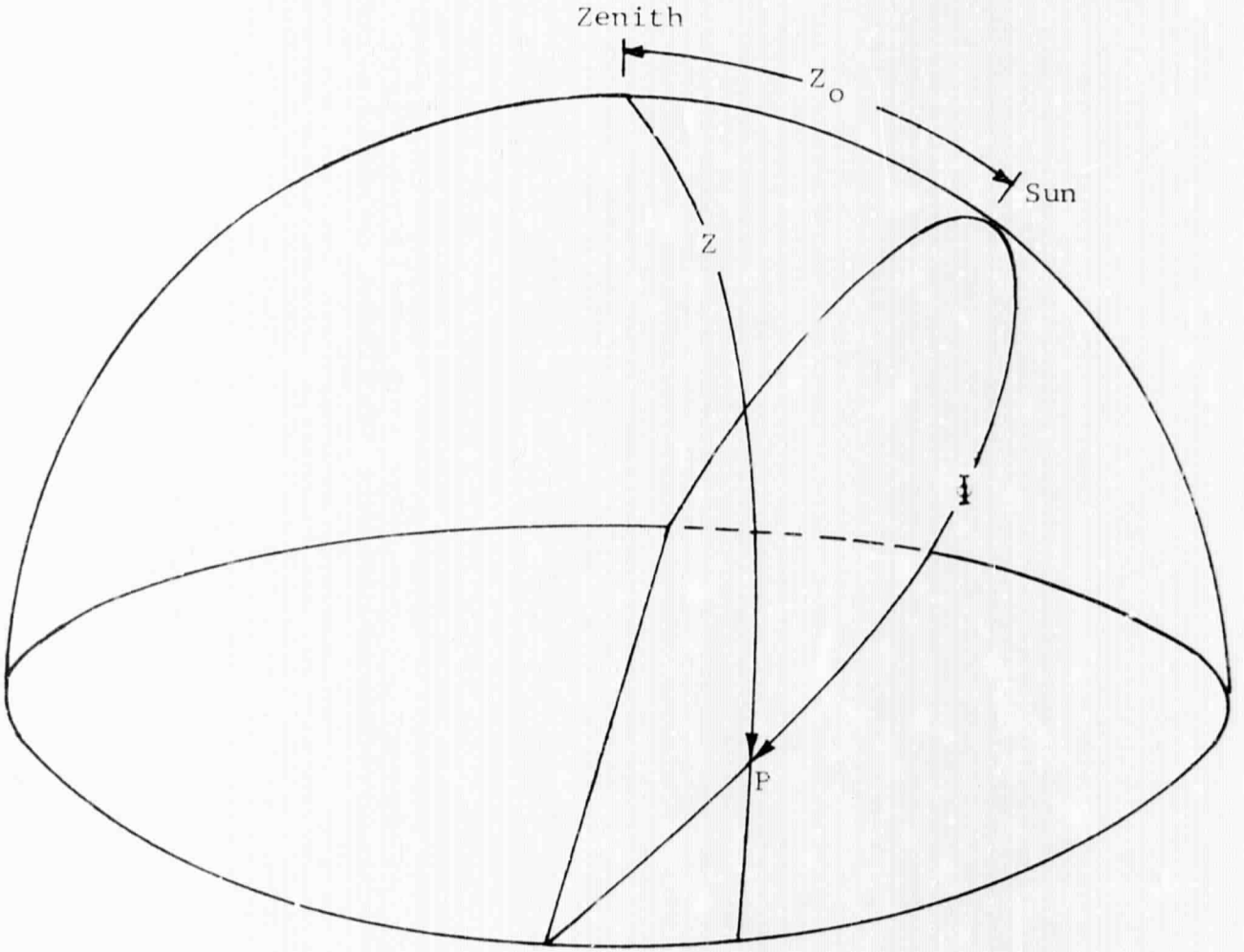


Fig. 3 Relationship Between the Zenith Angles and the Scattering Angle on the Celestial Sphere

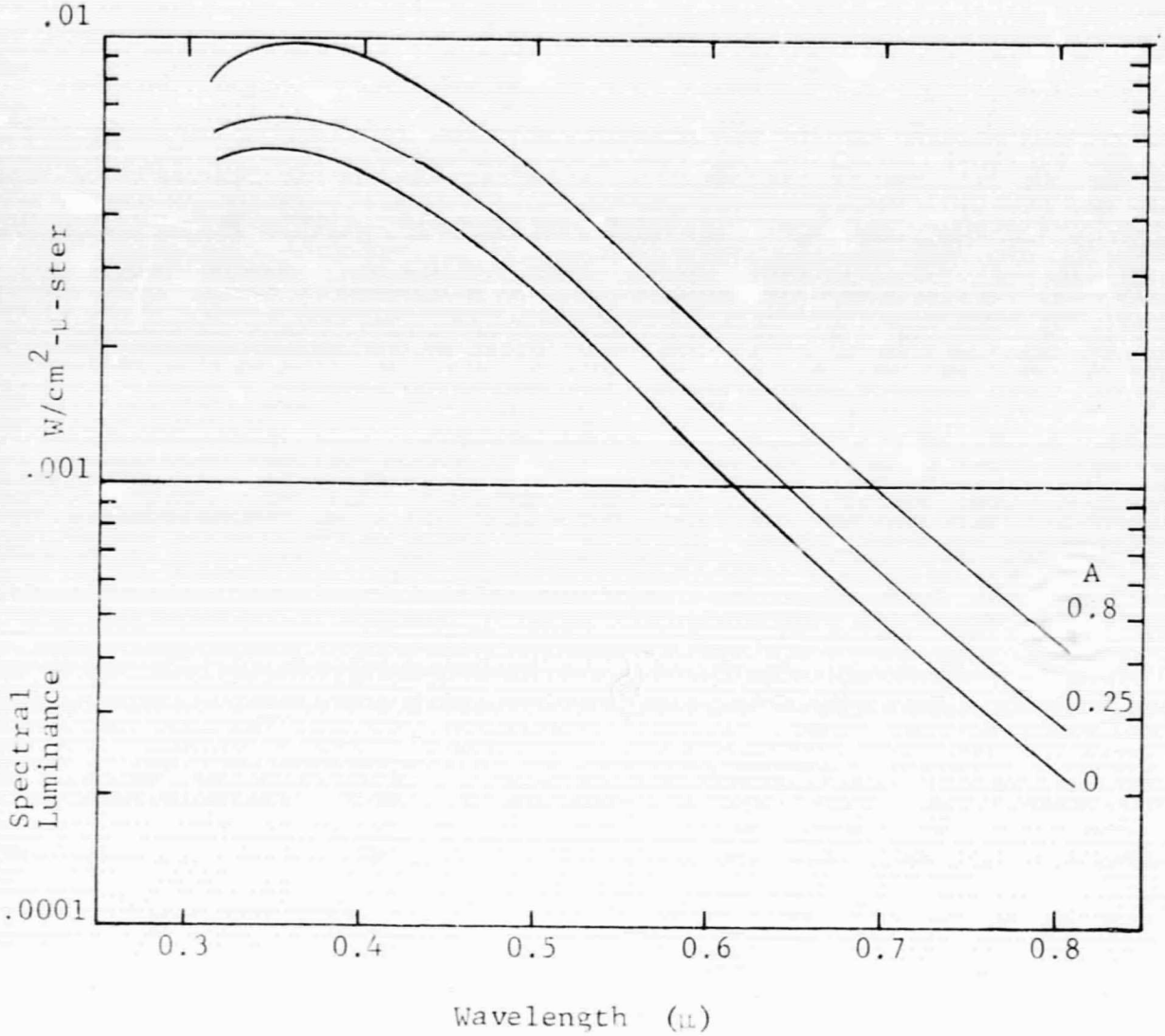


FIGURE 4. EFFECT OF SURFACE REFLECTANCE ON SKY SPECTRAL LUMINANCE

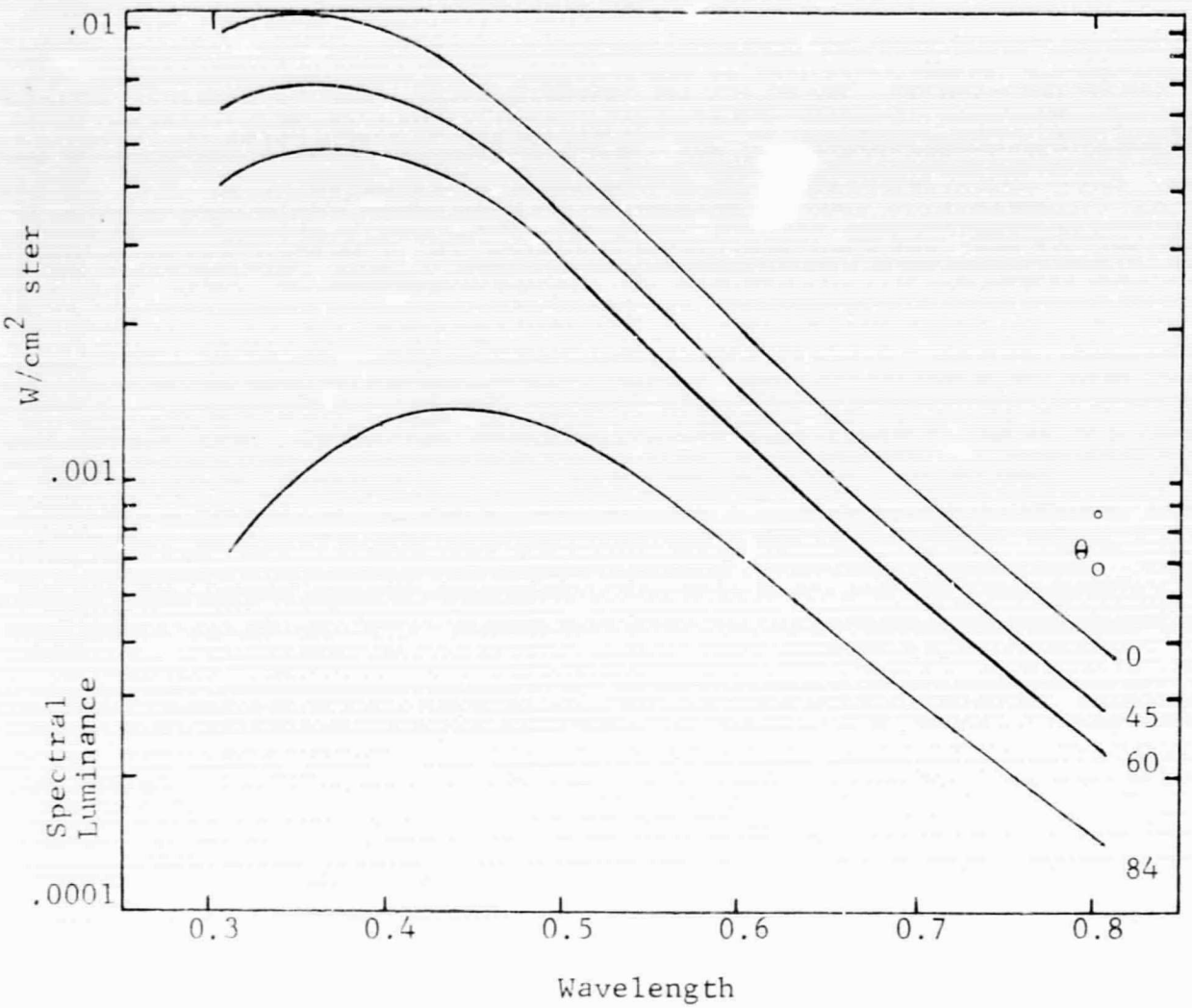


Fig. 5 Effect of Solar Zenith Angle on Sky Spectral Luminance

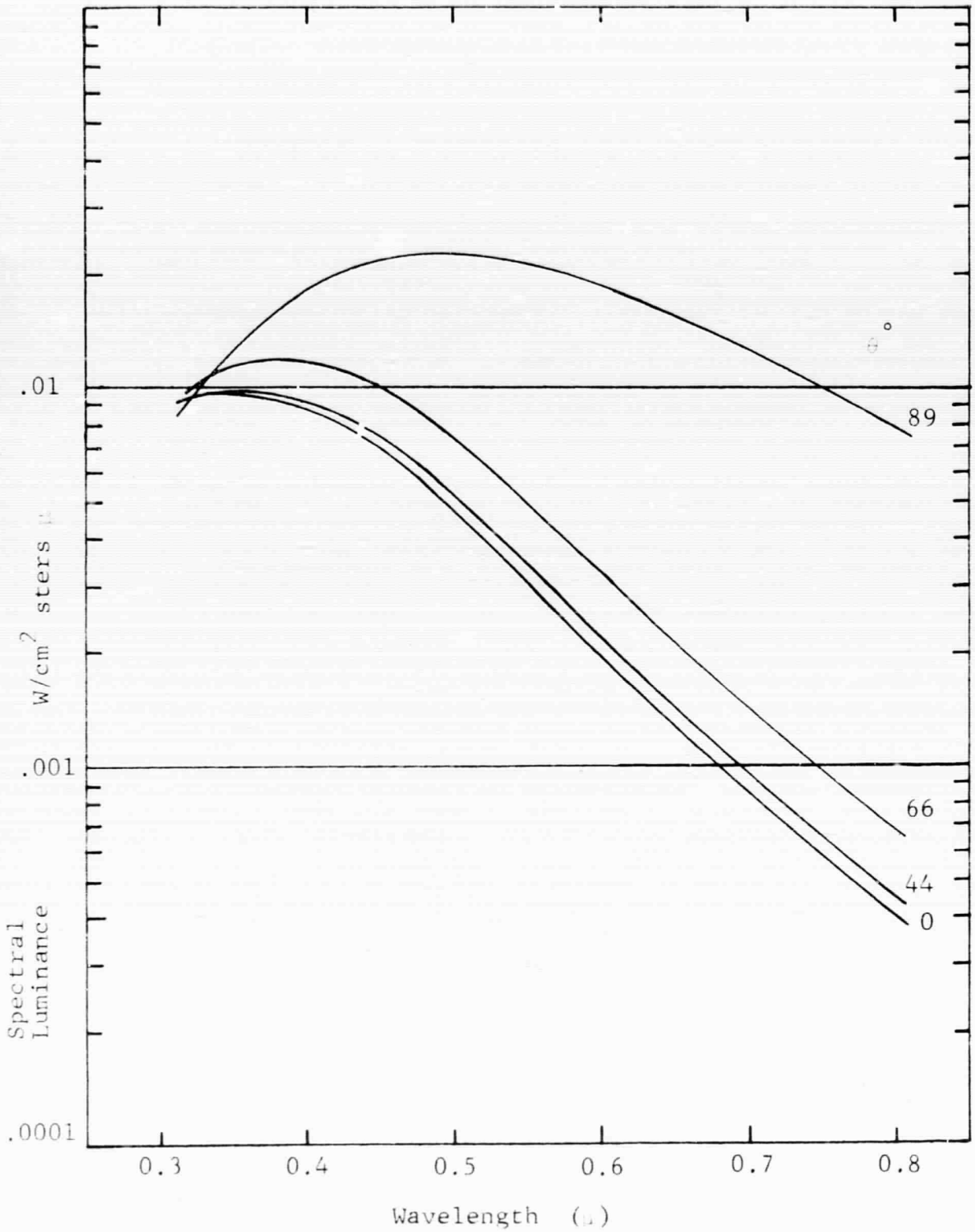


FIGURE 6. EFFECT OF OBSERVATIONAL ZENITH ANGLE Θ_o ON SKY SPECTRAL LUMINANCE

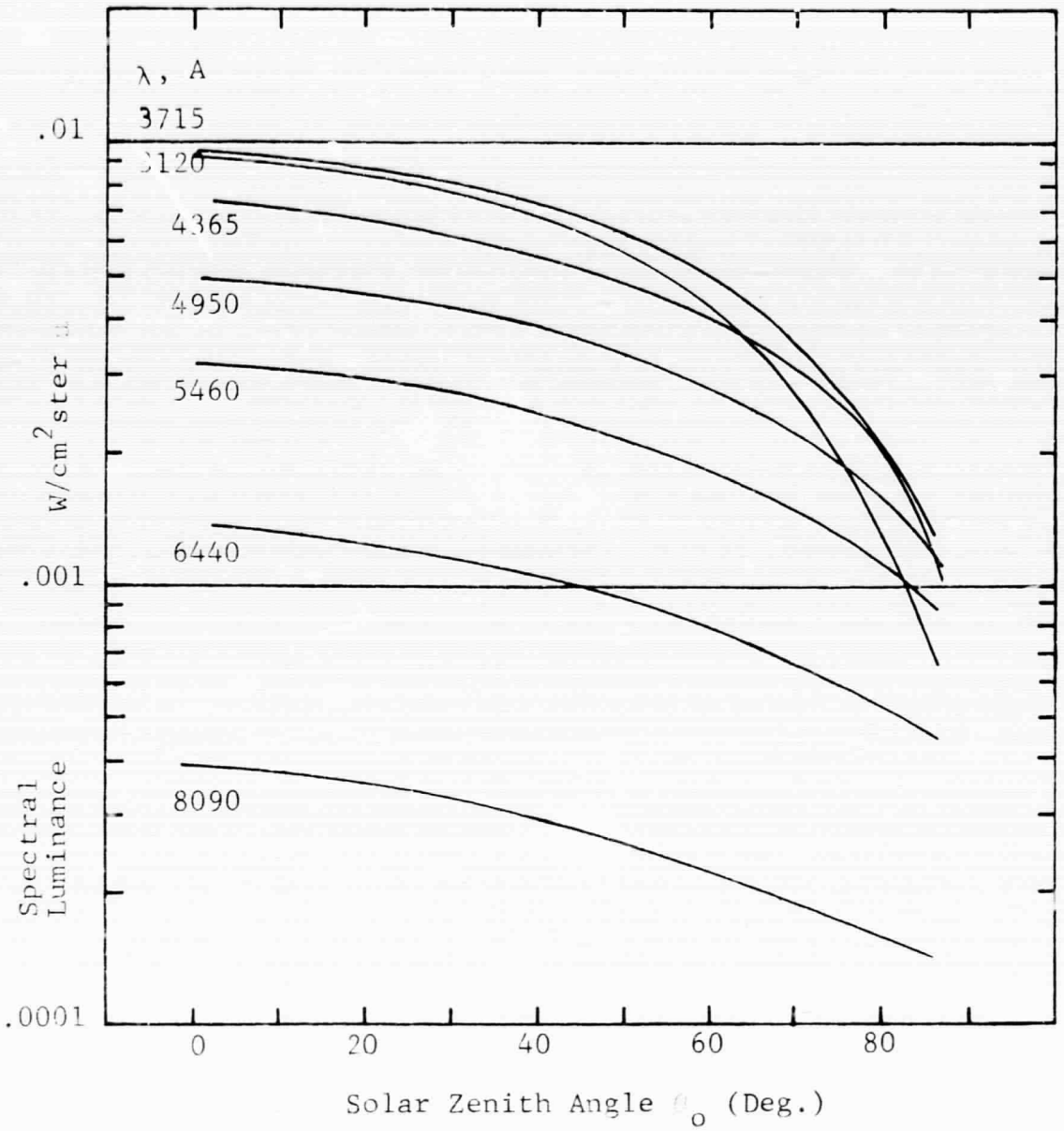


FIGURE 7. EFFECT OF WAVELENGTH λ ON ZENITH LUMINANCE vs. SOLAR ZENITH ANGLE

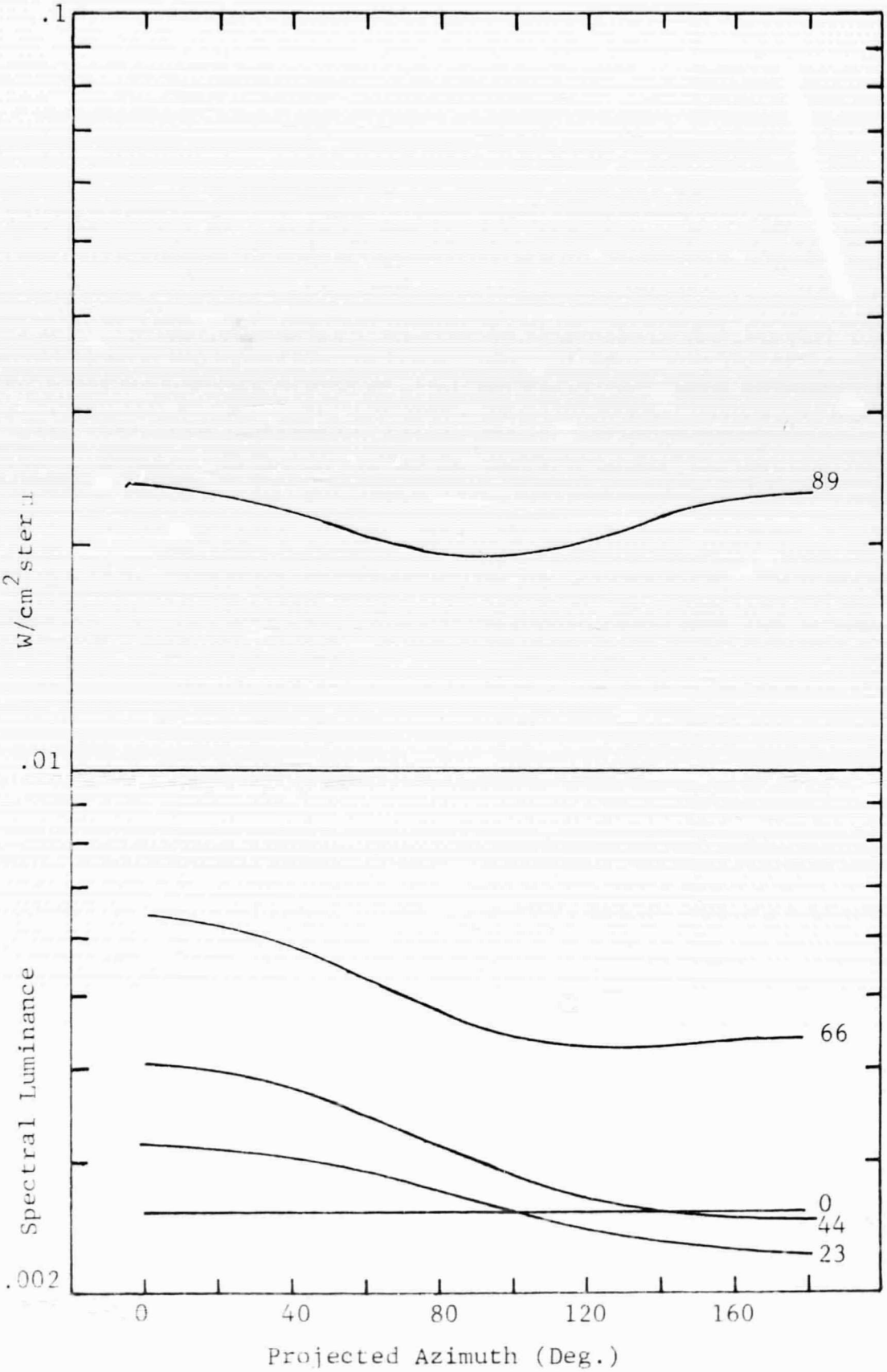


FIGURE 8. EFFECT OF PROJECTED OBSERVATION ZENITH ANGLE ON SPECTRAL LUMINANCE vs. PROJECTED AZIMUTH; SOLAR ZENITH ANGLE θ_o = 37 degrees
λ = 0.55 μ

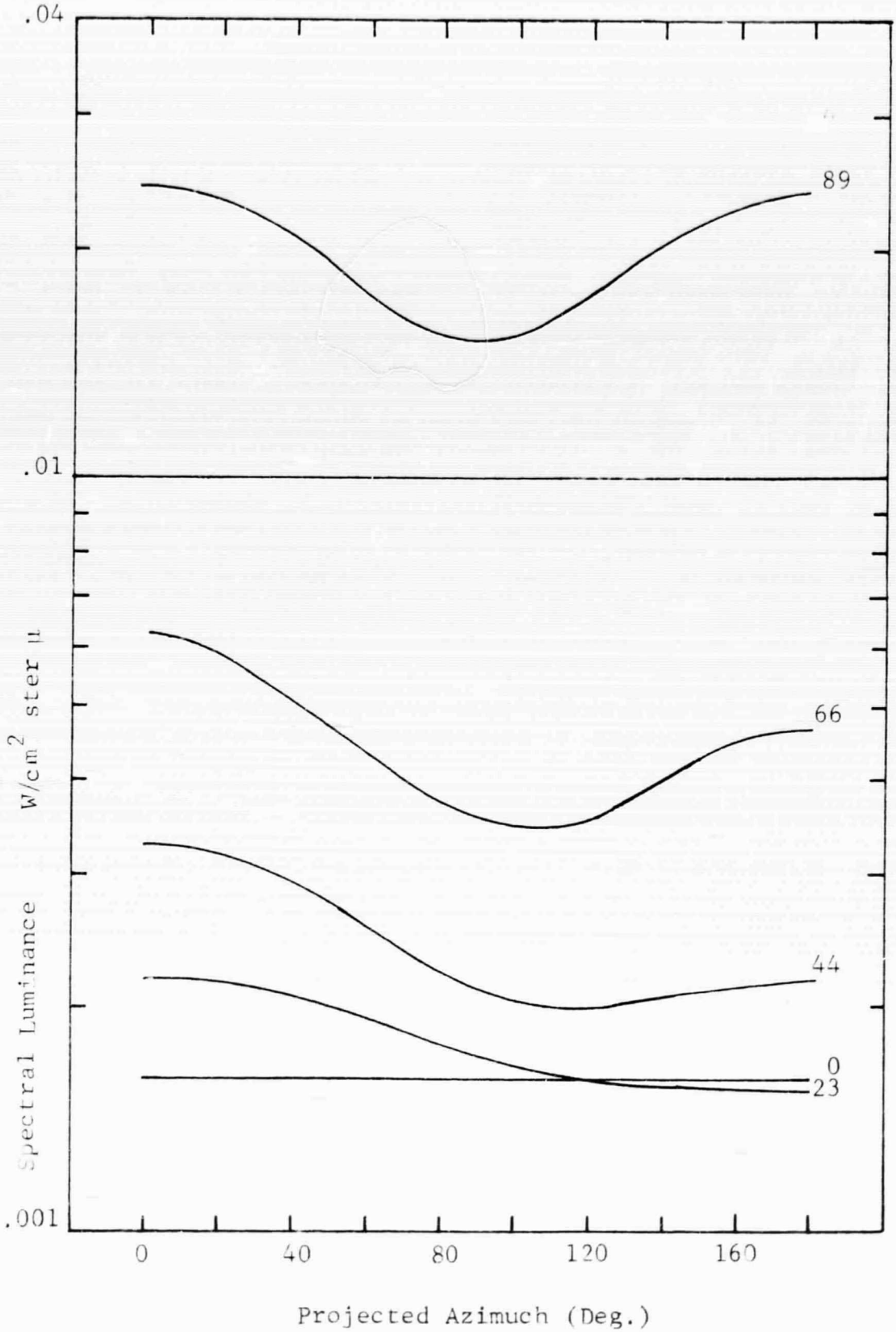


FIGURE 9. EFFECT OF OBSERVATIONAL ZENITH ANGLE θ ON SPECTRAL LUMINANCE vs. PROJECTED AZIMUTH
SOLAR ZENITH ANGLE θ_o = 66 degrees
λ = 0.55 μ

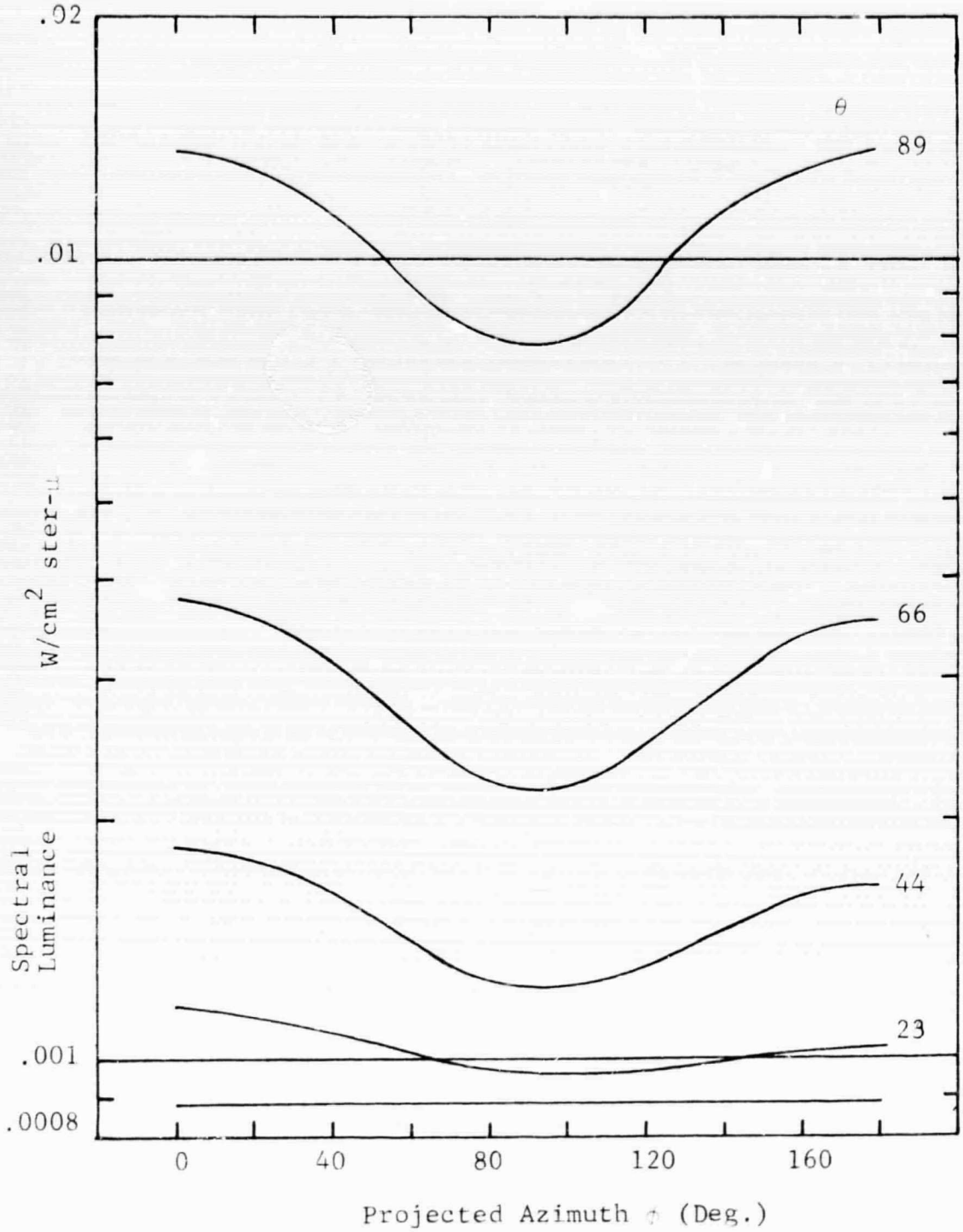


FIGURE 10 EFFECT OF OBSERVATIONAL ZENITH ANGLE θ ON SPECTRAL LUMINANCE vs. PROJECTED AZIMUTH λ = 0.55 μ

TABLE I MEAN SOLAR SPECTRAL IRRADIANCE VALUES

Wavelength, micron	Spectral Irradiance $w/cm^2/\mu$
0.312	0.0772
0.3715	0.1314
0.4365	0.1852
0.495	0.2050
0.546	0.1966
0.644	0.1661
0.809	0.1174

0.3μ to 0.8μ results in a 50 fold decrease in luminance. Because radiance is not highly dependent on surface reflectance, the remainder of the figures were drawn for surface reflectance A = 0.25.

Figure 5 shows zenith spectral luminance at selected solar zenith angles. For the sun near the horizon, a much larger change in spectral luminance versus zenith angle occurs for wavelengths less than 0.45 micron than for longer wavelengths.

Figure 6 shows spectral luminance away from the zenith for the symmetrical case of a zenith sun. The variation is less than 10 percent down to 45 percent from the zenith, but rises by a factor of 10 in the red and near-infrared as the horizon is approached. There is negligible variation near 0.35 micron, and a slight decrease at 0.30 micron. The maximum sky spectral luminance at a 0.25 value of surface reflectance, 0.022 w/cm^2-μ-ster, occurs at the horizon at 0.5 micron. The highest value 0.041 w/cm^2-μ-ster, occurs for reflectance A = 0.8, θ_o = 23°, θ = 89°, and ϕ = 0°.

Figure 7 expresses the same information as Figure 3 with solar zenith angle rather than wavelength as the independent variable. This plot more directly describes variation with time of day. Blue darkens more rapidly than red with approaching sunset, a conclusion not immediately evident from Figure 3.

Figures 8, 9 and 10 show the variation of sky spectral luminance with azimuth angle that occurs when neither solar nor observation angle is zero. Figure 8 shows that even with θ_o only 37°, spectral luminance varies by a factor of 1.5 with azimuth, and for θ_o = 66° and 84°, the variation is less than a factor of two. These curves were drawn for 0.546 micron wavelength.

In summary, the spectral luminance at the energy peak (0.55 micron) in the absence of aerosol scattering may be as low as 0.0017 w/cm^2 ster -μ at zenith for a clear winter noon at

latitude 42° (θ_o = 65°), as high as 0.020 w/cm^2 ster-μ at the horizon for a summer noon, and up to 0.04 w/cm^2 ster-μ at shorter wavelengths. The spectral luminance decreases by a factor of 1.5 to 2 at 90° from the solar azimuth and returns at 180°.

Consideration of the wavelength sensitivity of atmospheric scattering processes in both Rayleigh and particulate scatter is also required. Average measured sky spectral luminance as a function of wavelength in the visible is illustrated in Figure 11. The change in "color" of the sky with changing solar zenith angle and with pointing angle was illustrated previously in Figure 5 and 6. In the visible region there is little reason to pick one wavelength over another except to minimize the angular dependence of brightness and to maximize the source of scattering by the Rayleigh mechanism as opposed to particulate scatter or vice versa. The significant wavelength effects come into play when changes of detector altitude from the troposphere to satellite altitudes occur.

In addition to the scattered sunlight probing signal source in the troposphere, the action of the troposphere extinction fluctuations upon a signal must be considered. Just as scattering is the most important daytime source of probe signal in the troposphere, scattering is the most important extinction process. Over-all extinction throughout the troposphere must be computed for each geometrical path configuration using the appropriate model atmosphere. However, the altitude variation and the spectral variation of the extinction coefficient provide a simple input to the description of the overall problem. Figure 12 (from data in Ref. 12) illustrates the altitude variation of the extinction coefficient for two wavelengths and separates the Rayleigh scattering extinction coefficient from the particulate scattering. The coefficient for particulate scattering is for a nominally "clear" sky. Obviously the presence of ice crystals, man-made sources of air pollution, and other sources of atmospheric turbidity will greatly increase the values given herein. Again,

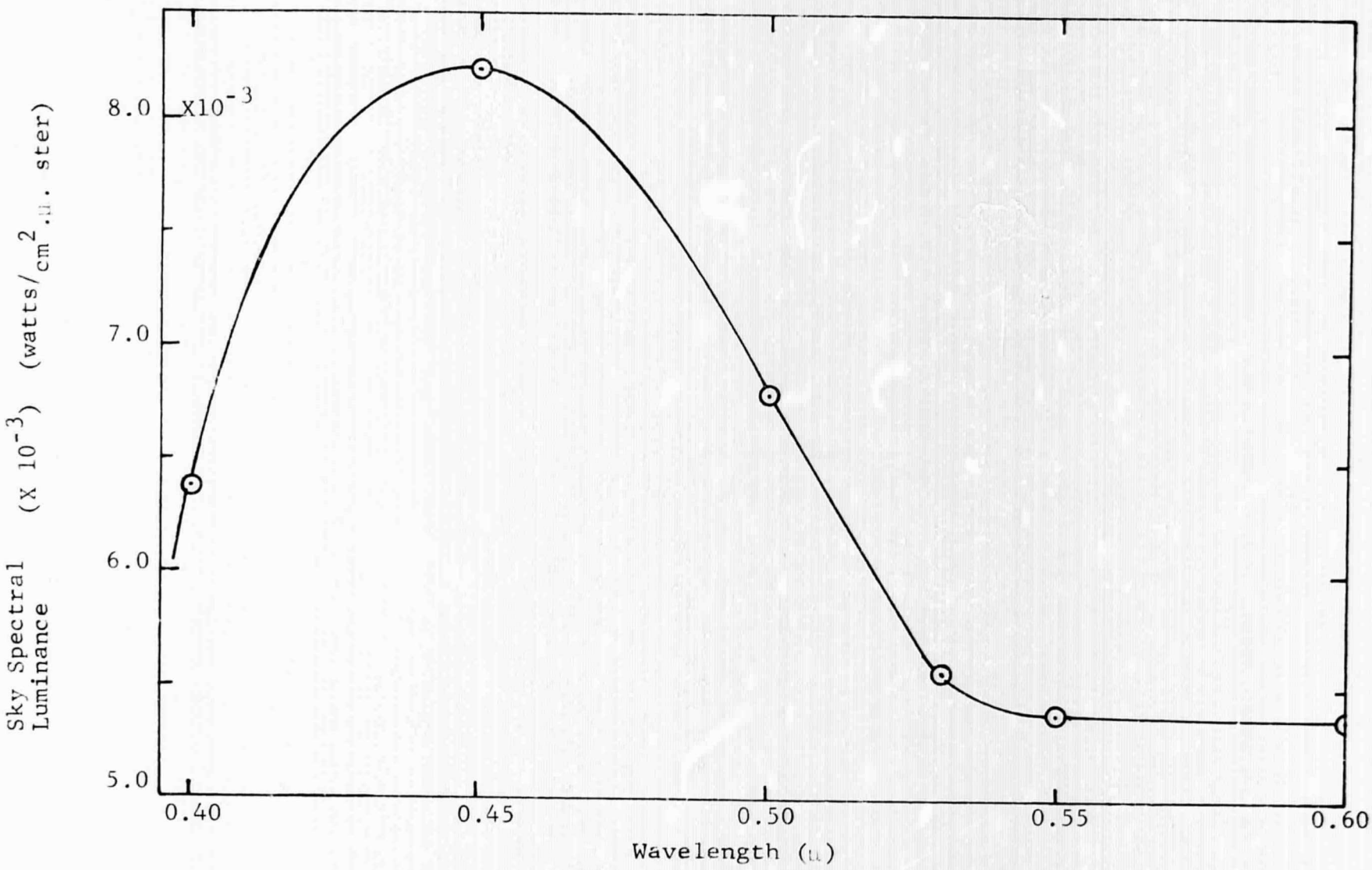


Fig. 11 Zenith Sky Spectral Luminance

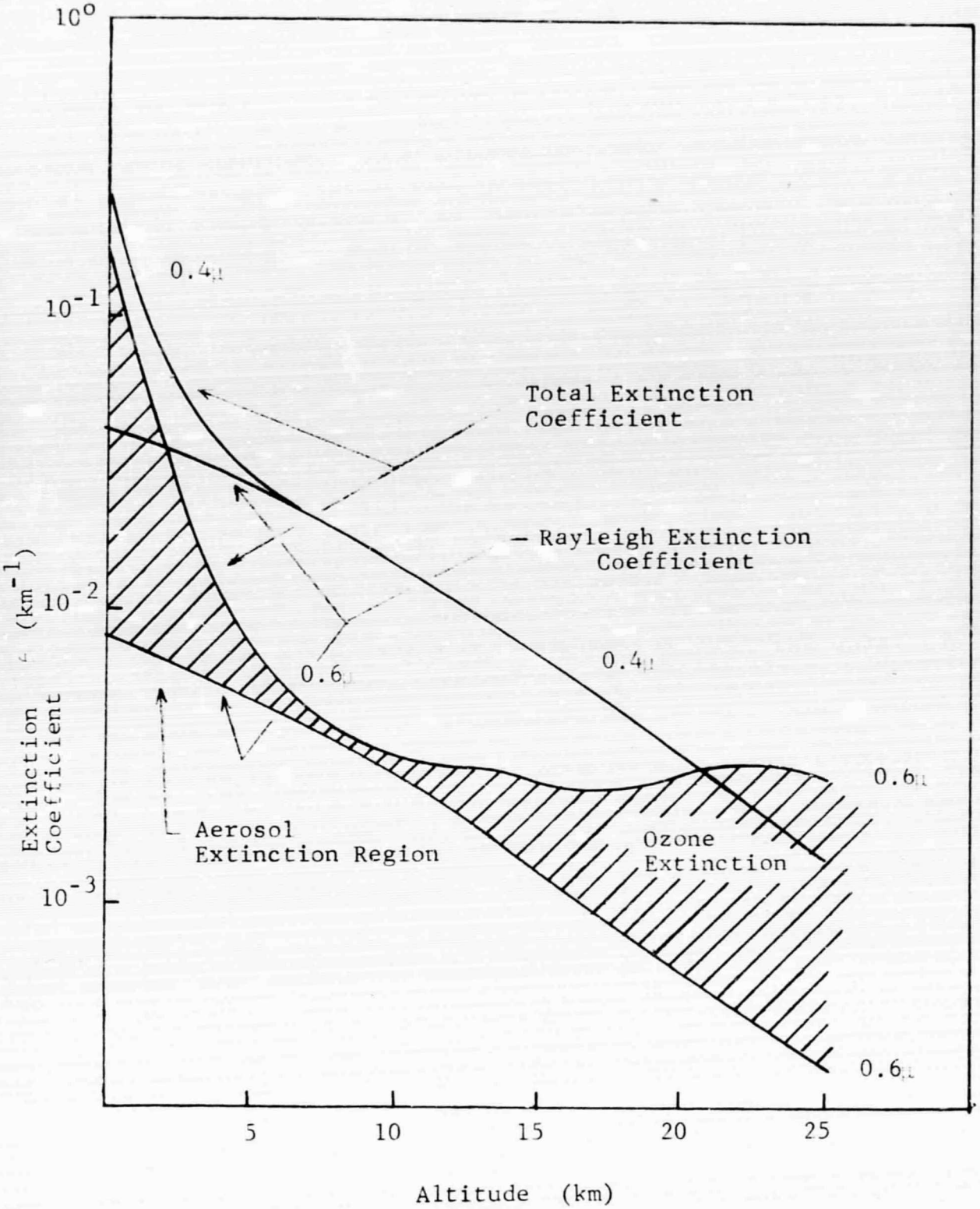


Fig. 12 Relative Contribution of Aerosol Scatter and Ozone Extinction to Total Extinction Coefficients

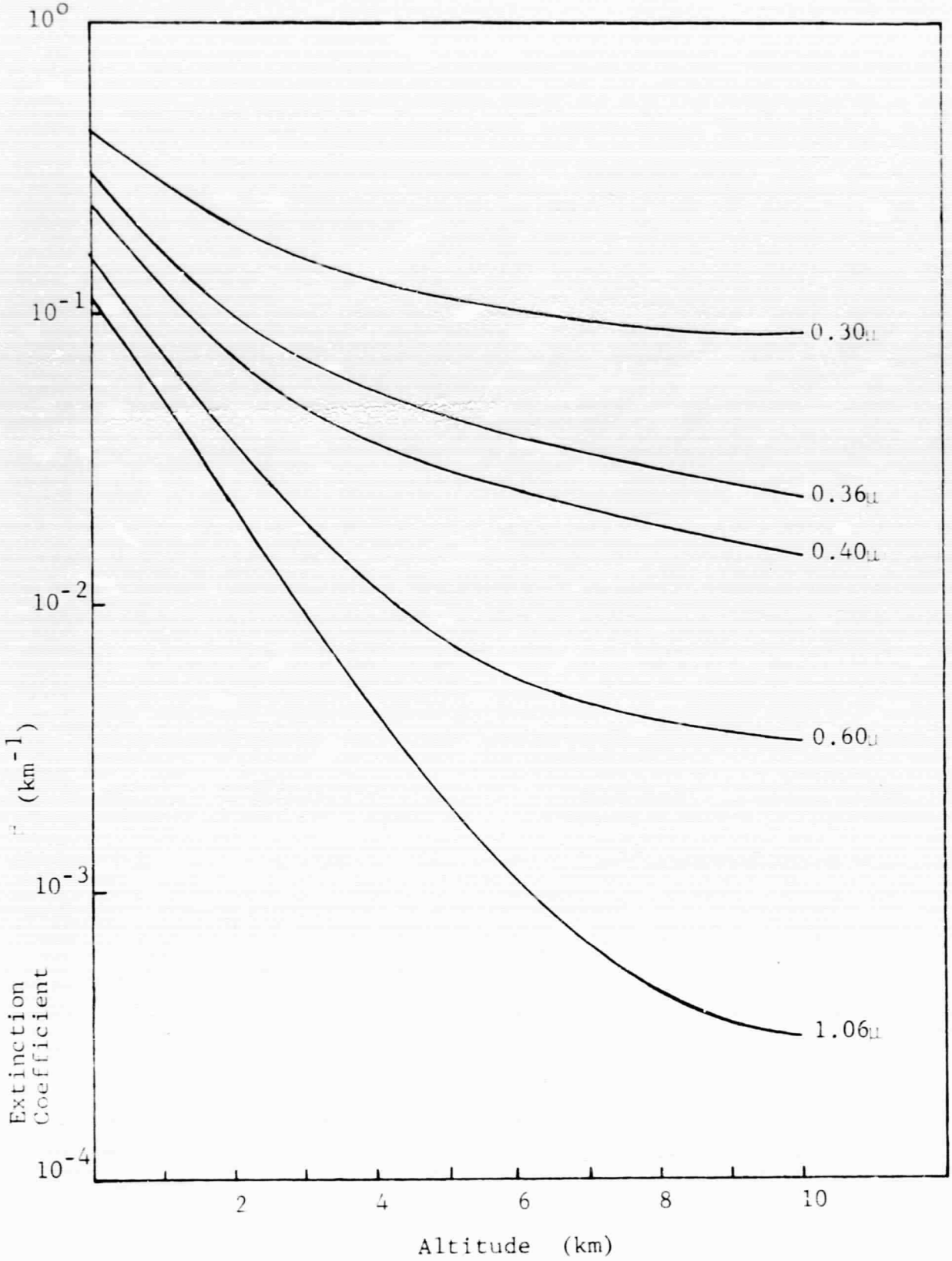


Fig. 13 Total Extinction Coefficients as a Function of Altitude and Wavelength

it is clear that for the lowest part of the troposphere, there is no definite advantage in choosing one wavelength region over another in the visible spectrum. However, if the cross beam experiment seeks to emphasize the extinction processes in one region of the lower atmosphere as opposed to another (in order to increase signal-to-noise ratio), then the altitude dependence of the extinction coefficient at different wavelengths must be considered. Figure 13 illustrates this in more detail for the lower part of the troposphere. It may be concluded that extinction of an external signal source is much more uniform over the troposphere in the blue region than in the near infrared. On the other hand, Figure 12 shows that the extinction coefficient in the red portion of the spectrum eventually exceeds that for the blue as altitude increases and the tropopause is passed.

The appearance of the sky in the nonvisible portion of the spectrum and its variation in spectral luminance with wavelength and altitude must be treated somewhat differently than for the visible region. Because scattering efficiency drops rapidly with increasing wavelength, scattering as a source of probing signal is not important for the infrared region. In the near ultraviolet, ozone absorption below about 3000 A becomes significant and these wavelengths are not useful for sensors below the peak of the ozone layer at about 20 to 30 km. At the ground, the greatest atmospheric effects in the infrared are a result of the absorption bands of atmospheric constituents. Figure 14 illustrates the absorption of the solar spectrum by molecular bands in the near infrared. Farther into the infrared, the solar spectrum is absorbed as before, but emission of thermal radiation becomes important. Figure 15 illustrates the correspondence in wavelength of absorption bands observed in the daytime and emission bands observed at night. Most of the important bands are attributed to ozone, molecular oxygen, carbon dioxide, and water vapor. The important band systems in the infrared attributable to atmospheric constituents are tabulated in Table II.[11] The comparison of

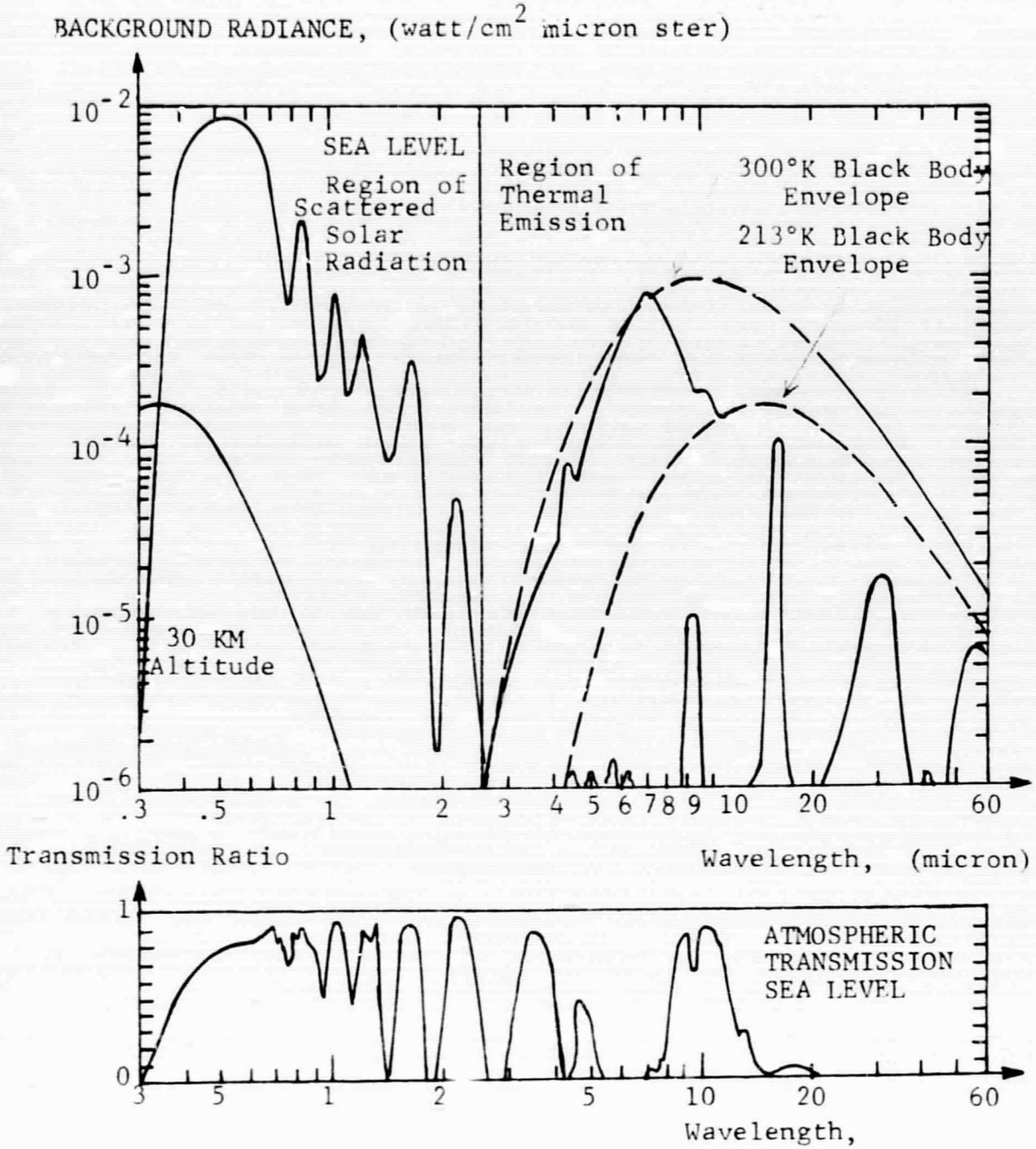


FIG. 14. EMISSION SPECTRUM OF ATMOSPHERIC RADIATION BACKGROUND FOR TWO ALTITUDES (From Ref. 16)

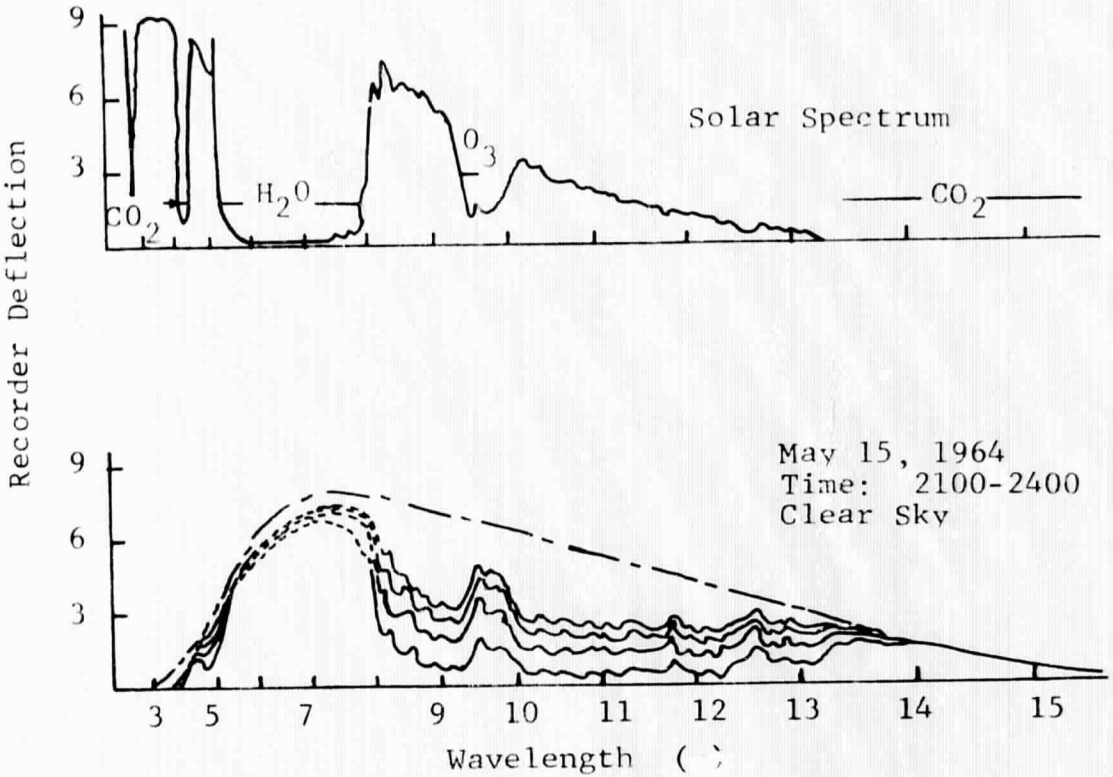


Fig. 15 Infrared Sky Spectrum Observed on a Clear Night. The Upper Curve Gives a Solar Spectrum for Comparison. (ref. 17)

TABLE II IMPORTANT ATMOSPHERIC INFRARED BANDS

CO_2 INFRARED BANDS

Band Center (cm^{-1})	Band Center (μ)	Integrated Absorption ($atm^{-1}\ cm^{-2}$)
2350	4.3	2706.0
3609	2.72	28.5
3716	2.69	42.3
668	14.97	240
667	15.00	
648	15.43	
618	16.18	
5109	1.96	0.43
4984	2.01	1.01
2137	4.70	0.15
2094	4.78	
2077	4.82	
1933	5.17	0.83
1896	5.30	
742	13.48	0.22
721	13.87	7.50
961	10.4	0.022
1084	9.4	0.053

WATER VAPOR BANDS

Band Center (cm^{-1})	Band Center (μ)	Integrated Absorption ($atm^{-1}\ cm^{-2}$)
1595	6.27	225 (1 + 0.05 T)
3652	2.74 *	191
3756	2.66	
3151	3.17	3.2
7252	1.38	15.6
6874	1.46	0.48
8807	1.10	1.9

OZONE INFRARED BANDS

Band Center (cm^{-1})	Band Center (μ)	Integrated Absorption ($atm^{-1}\ cm^{-2}$)
1042	9.6	455
1103	10.1	10.6
701	14.6	?

sea level sky radiance and that at 30 kilometers clearly shows the reduction of scatter and superimposed absorption bands at short infrared wavelengths. At longer wavelengths, above about 2.5 microns, the thermal emission from the atmosphere becomes more important than scatter, and, again, absorption bands are important at sea level. At the higher altitude, however, only thermal emission bands are present and are important to wavelengths greater than 60 microns. Correspondence of thermal emission peaks observed at 30 km altitude with the dips in atmospheric transmission at sea level in the infrared region shows that thermal emission may be usable as a probing signal for a high-altitude sensor whereas extinction by lower altitude processes would cause added modulation to appear on the probe signal.

The ultraviolet region as a source of probing signals is much more restricted than either the visible or the infrared because the atmosphere becomes transparent to ultraviolet below 3000 A only above about 30 km. The shorter wavelengths which cause ionization and dissociation of molecular species have a unit optical depth in the atmosphere at even higher altitudes. Figure 16 illustrates the altitude at which unit optical depth occurs as a function of ultraviolet wavelength. It is easily seen that over much of the ultraviolet spectral range, only satellite measurements looking downward are feasible because the atmosphere is still optically thick looking upwards from typical balloon altitudes (35 km) and is optically thin looking upwards from typical satellite orbital altitudes (400 km).

The characteristics of the lower atmospheric sources of probing signals may be related to the parameters of cross beam experiments and are especially useful in defining the region which may be observed from either the ground or from satellite orbital altitudes as a function of the wavelength of observation. These applications are summarized in Table III.

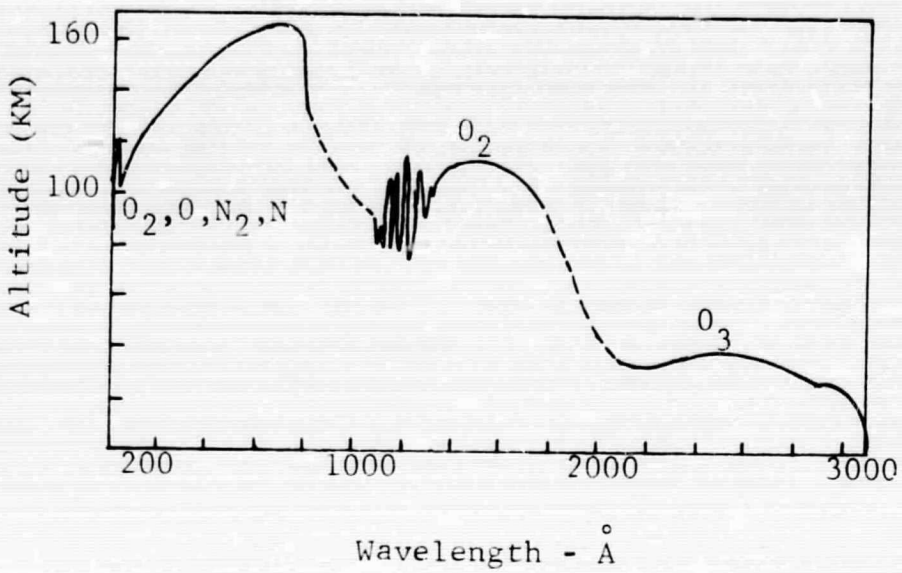


Figure 16 Altitude at Which Solar Ultraviolet Radiation is Reduced to a value of e^{-1} of its Original Intensity (Ref. 18)

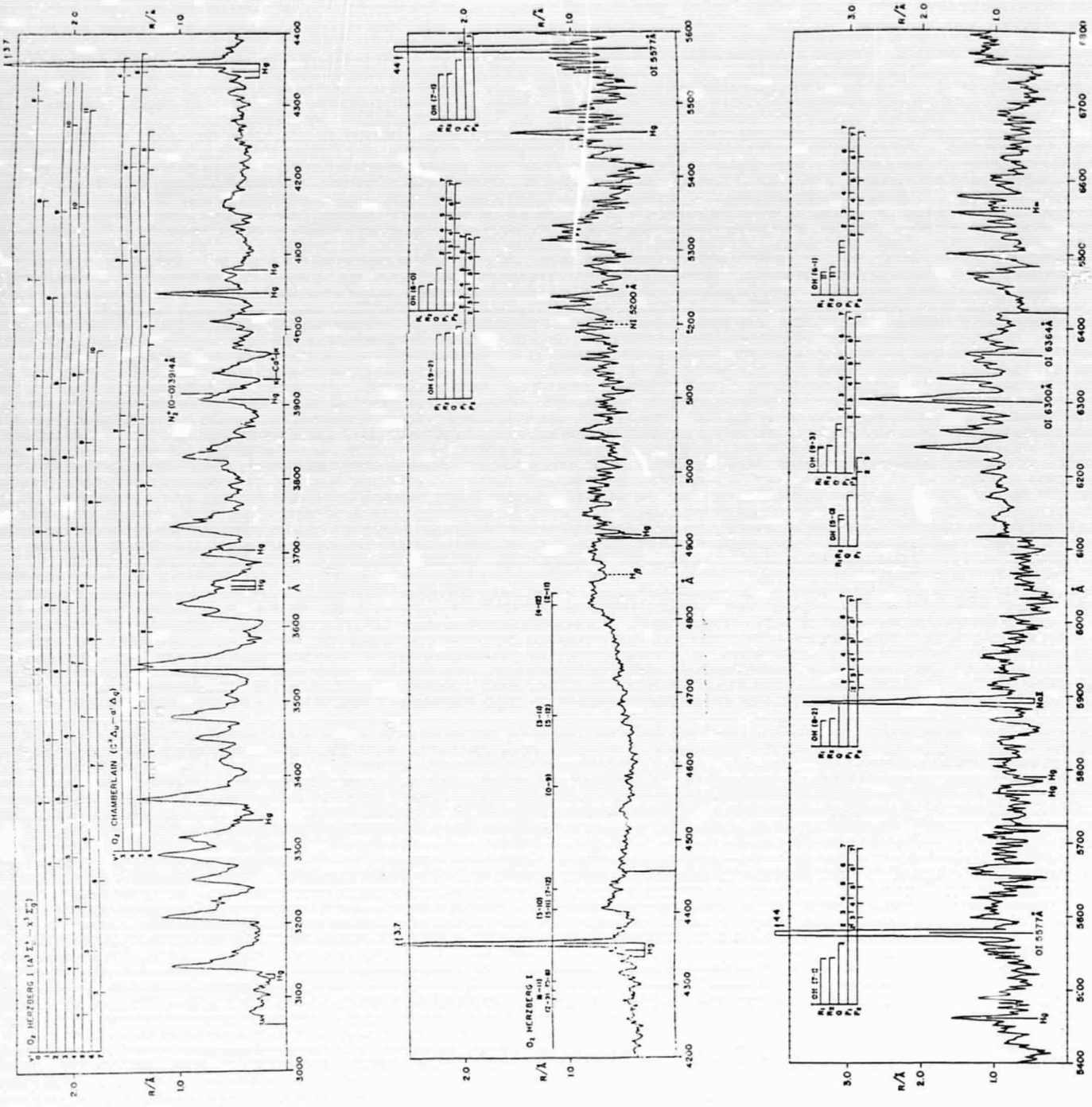
TABLE III APPLICATIONS OF LOWER ATMOSPHERIC SCATTERING, EMISSION, AND EXTINCTION SOURCES TO CROSS BEAM SYSTEM

Optical Wavelength	Sky Maximum Luminance Spectral ($w/cm^2ster\text{-}\mu$)	Sky Minimum Spectral Luminance	Parameter Making Greatest Variation in Luminance	Measurement Region	Detector Location	Orientation	Scatter or Extinction Process
0.3				30 km	Satellite	Downward	Rayleigh
0.4	1×10^{-2}	6×10^{-4}	Solar Zenith Angle	0 to14 km, Troposphere	Satellite	Downward	
				0 to14 km, Troposphere	Ground	Upward	Rayleigh plus Aerosol
0.6	2×10^{-2}	2×10^{-3}	Observational Zenith Angle	Troposphere, 0-7 km	Satellite	Downward	Rayleigh + Aerosol
				Ozonosphere 20-40km	"	"	Ozone Extinction
				0 to 7km, Troposphere	Ground	Upward	Rayleigh + Aerosol Scatter
Infrared Bands	7×10^{-4}	1×10^{-6}	Integrated Absorption & Density of emitting, scattering, or absorbing species, ie Ozone, water vapor, or carbon dioxide.	Troposphere 0 to 20 km	Ground	Upward	Water Vapor Scatter and Extinction
				Troposphere 0 to 20 km	Satellite	Downward	Water Vapor Scatter and Thermal Emission
				Ozonosphere	Satellite	Downward	Ozone Scatter
				Ozonosphere 20-40 km	Ground	Upward	Ozone emission and/or extinction

From the standpoint of a ground based cross beam experiment, the overall signal level defined by the spectral luminance of the sky, its range of values, and the major experimental factor which affect the signal level have been outlined. It is apparent that in the visible region, selection of either the blue or red end of the spectrum allows one to minimize the effects of either observational zenith angle or of solar zenith angle respectively. In both cases, the change in overall signal level caused by azimuthal variation in beam direction will be small compared with zenith angle effects.

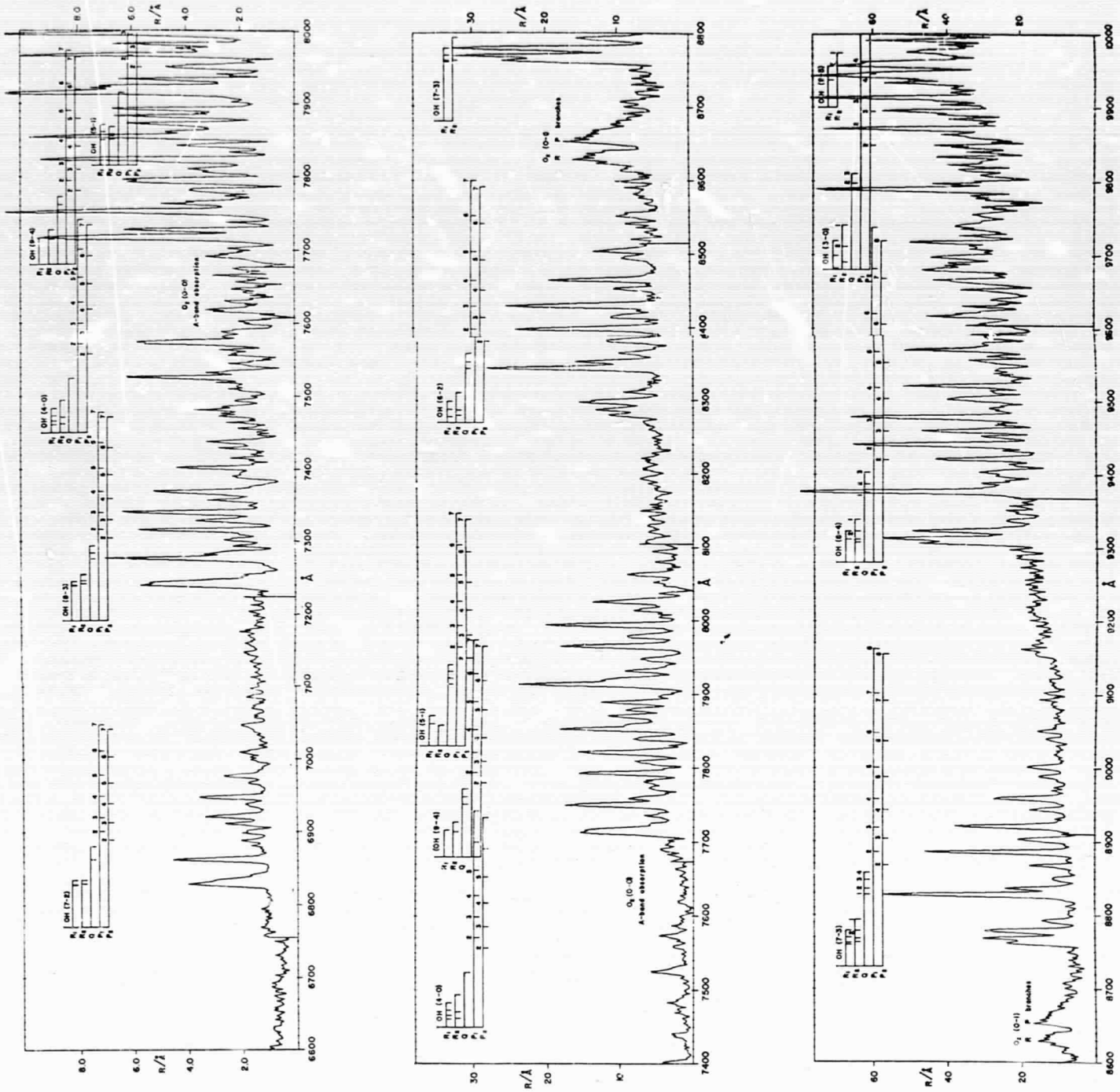
B. Nonthermal Radiation from the Upper Atmosphere

Most of the energy emitted in the visible, near infrared, and ultraviolet spectral regions by the upper atmosphere is nonthermal in nature; that is, it is emitted from states which are not in thermal equilibrium with their surroundings. The energy from a given spectral region is usually appreciably higher than that which would be emitted by a blackbody radiator at the kinetic temperature of the gas, and the spectral distribution of emission is distinctly non-Planckian. Nonthermal processes which contribute to this emission include resonant scatter, resonant fluorescence, Rayleigh scatter, Mie scatter in the daytime, and a variety of chemical and electronic excitation processes which contribute to the night airglow. The night sky airglow spectrum as observed from the ground[19] is illustrated in Figure 17. Two important characteristics of the source of nonthermal emission are their altitude distribution and their intensity. If one is given a source of sufficient intensity to make it appear to be a feasible probing signal, the altitude of its emission then becomes the pertinent factor. If we are interested mainly in tropospheric problems such as meteorology, then it is appropriate to consider only sources of emission (or extinction) which are localized to the troposphere because then the total effective beam length will be reduced. On the other hand, if ionospheric measurements are



FOLDOUT FRAME #1

Fig. 17 Night Sky Emission Spe



pectrum 0.3 to 1.0 micron (ref. 19)

FOLDOUT FRAME #2

of interest, or those in the mesosphere, it is appropriate to choose emission sources which are not only localized to these regions but which will have the minimum reaction in the remainder of their path to either the satellite or the ground-based detector. A ground-based ionospheric cross beam measurement utilizing a visible nonthermal radiation as a probing signal would suffer tropospheric scatter and extinction effects. An alternative experiment could consist of a satellite-based measurement of an ultraviolet nonthermal emission feature for which the optical path below some calculable altitude would become opaque.

In addition to absolute intensity and altitude distribution, the intensity of the sources with respect to background emissions in the same spectral range are important. For example, in the daytime the dayglow nonthermal emissions are superimposed upon a brilliant scattered sunlight background. Thus the problem becomes one of separating a low-intensity line emission feature from the background Fraunhofer solar spectrum. Various techniques have been developed to accomplish this,but the technological feasibility of their application to the cross beam remote-sensing technique appears to be questionable at present. However, scattering in resonance or resonance fluorescence lines appears as a strong feature of the twilight sky and may provide a suitable tool for some upper atmospheric studies. At nighttime the nonthermal emissions which are important appear to be much more intense than the background continuum from the sky including zodiacal light, gegenschein, continuum airglow, and starlight. Scattered moonlight presents a background problem, however, and the presence of added scattering centers such as salt spray or dust in the troposphere creates even more background noise.

The problem of separation of a desired spectral line emission feature from a continuum-like background may be formulated in terms of a signal to noise ratio incorporating the total line intensity, the background spectral intensity and the

passband of the optical system. The signal is the intensity of the emission line expressed as the spectral intensity multiplied by the gaussian linewidth at half maximum. The noise or background signal intensity is defined by the continuum emission spectral intensity multiplied by the input passband of the instrument. Insofar as narrow band interference filters may be used to reduce the spectral passband of the optical detector, it is apparent that for a given emission line and given background conditions, the passband of the filter will control the signal to noise ratio.

For a typical airglow line intensity of 300 R($=10^{-10}$ w/cm^{2}ster), the signal to background ratio may be plotted over a range of background scattered light intensities from the lower limit of the starlight plus zodiacal light intensity to the upper limit of full daylight. The passband values of the optical filters are parametric in the illustration of this relationship in Figure 18. It is clear that as the filter bandwidth decreases to the limit of the gaussian line width, the signal to background ratio is still below unity during full daylight. In fact, the value of I_s/I_b in full daylight is approximately 10^{-4}. On the other hand, selection of a suitably narrow bandwidth during nighttime conditions allows reasonable probe signal intensity to background intensity ratios to be maintained even during full moonlight. However, current practices in airglow measurement usually limit operations between the last quarter to first quarter phases of the moon.

Evaluation of the utility of upper atmospheric nonthermal emission features for cross beam probing signals is not quantitatively possible with the possible exception of the atomic oxygen emission features at 5577 A and 6300 A. In general these two emissions have been studied in enough detail that their temporal and spatial characteristics are reasonably well known, as well as the altitude range of their emission. The known characteristics of a number of airglow spectral features are presented in Table IV with an evaluation of their applicability to cross beam experimental variables. In each case of emission

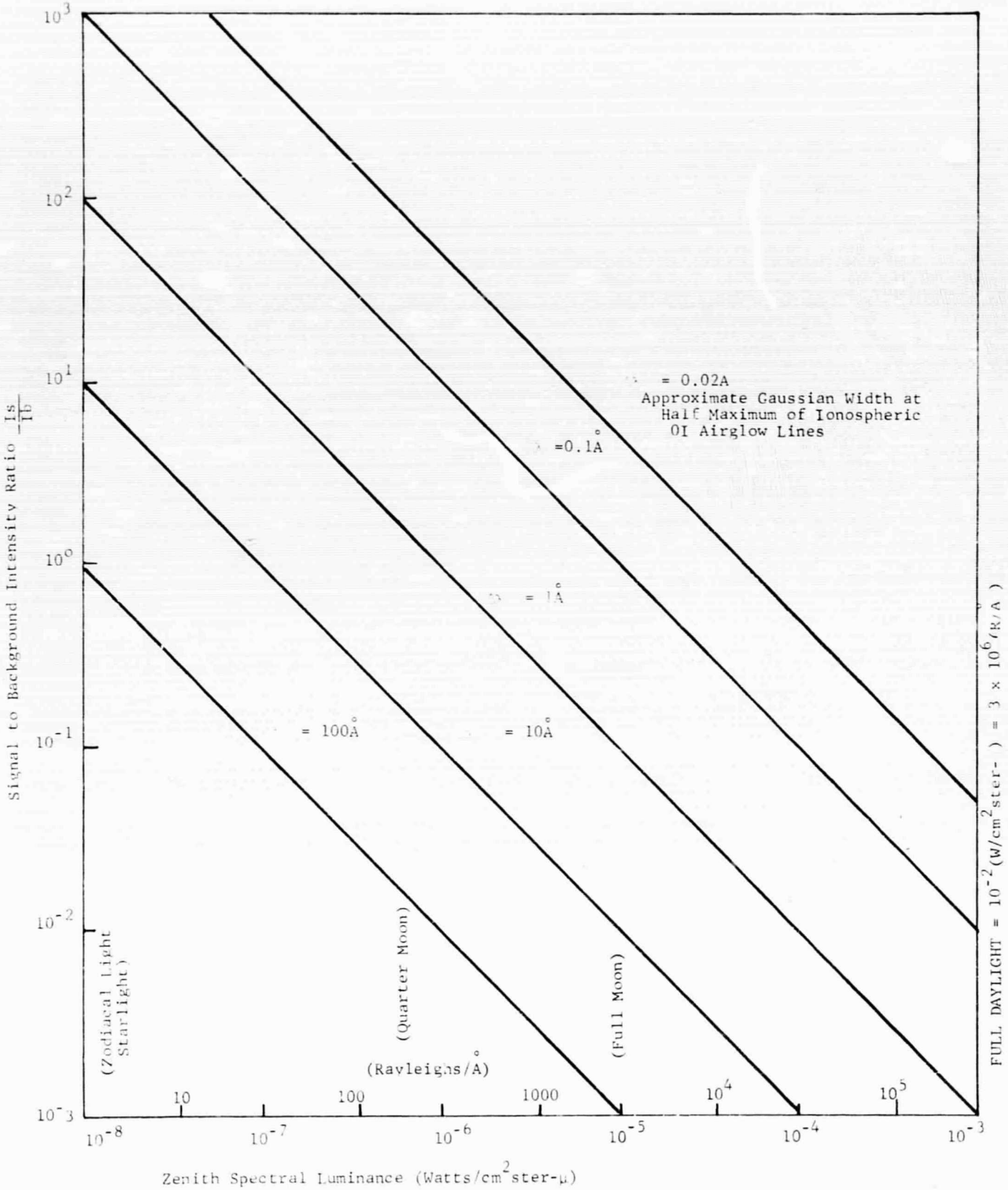


FIGURE 18 RATIO OF LINE INTENSITY TO BACKGROUND INTENSITY vs. ZENITH SPECTRAL LUMINANCE FOR PARAMETRIC VALUES OF FILTER PASSBANDS I_s = 300R = 1 X 10^{-10}(W/cm^{2}ster)

TABLE IV APPLICATION OF UF

Spectral Feature			Intensity (R)			Altitude (Km)	Background (R/A)		
λ	Specie	Transition	Night	IBC III Aurora	Day		Night Continuum	Line or Band	Day Continuum
5577	OI	$^1D_2 \rightarrow {}^1S_o$	¶250	10^4 10^5	$< 2 \times 10^4$	100	3	2 (±) OH(7.1)	3×10^7
6300	OI	$^3P \rightarrow {}^1D_2$	150	5×10^4	1×10^3	260	3	6 (=) OH(9.3)	2×10^7
8629	O_2	$b\,{}^1\Sigma_g^+ \rightarrow X\,{}^3\Sigma_g^-$ (0,1)	1.5×10^3	4×10^5		97	---	-- (±)	1×10^7
8659	O_2								
1.58 μ 1.466 *	O_2	$a\,{}^1\Delta g \rightarrow X\,{}^3\Sigma_g^-$ (0,1)	2×10^4	10^6			---	100 (3,1) OH(4,2)	1×10^6
5199.42	NI	$^4S^\circ_{3/2} \rightarrow {}^2D^\circ_{5/2,3/2}$	5	10^3			3	0.1 (-) OH(9,2)	4×10^7
3914.4	N_2^+	$B\,{}^2\Sigma_u^+ \rightarrow X\,{}^2\Sigma_g^+$ (0,0) IN	1×10^3	2×10^5	3×10^4		0.5	--- (+)	1×10^8
4278.1	N_2^+	$B\,{}^2\Sigma_u^+ \rightarrow X\,{}^2\Sigma_g^+$ (0,1) IN					0.5	--- (+)	1×10^8
1.051 μ	N_2	$B\,{}^3\Pi_g \rightarrow \Delta\,{}^3\Sigma_u^+$ (0,0) IP		2×10^6			---	20 (+) OH(4,1)	5×10^6
8912.4	N_2	$B\,{}^3\Pi_g \rightarrow \Delta\,{}^3\Sigma_u^+$ (0,1) IP					---	50 (+) OH(7,3)	
6562.82	H_α	$^2P^\circ \rightarrow {}^2D$	10	6×10^3			3	6 (+) OH(6,1)	2×10^7
4861.33	H_β	$^2P^\circ \rightarrow {}^2D$	5	3×10^3			1	--- (±)	6×10^7
2.801 μ	OH	$X\,{}^2\Pi$ (1,0)				85			5×10^4
1.668 μ		(5,3)						---	
1.582 μ		(4,2)	1×10^5					---	1×10^6
1.505 μ		(3,1)	1.5×10^5					---	
1.290 μ		(8,5)	5×10^4					---	
1.212 μ		(7,4)	5×10^4					---	
8824 *		(7,3)						---	1×10^7
8342 *		(6,2)						---	
7911 *		(5,1)						---	

OUT FRAME #1

APPLICATION OF UPPER ATMOSPHERE NON-THERMAL EMISSION TO CROSS BEAM EXPERIMENTS

(R/A)	Day Continuum	Range of Intensity Variation	Type of Variation	Baseline of Cross Beam System	Approximate Range Nighttime Signal to Noise Ratio$\Delta\lambda$= 1A
±)	3×10^7	~ 100%	Temporal and Spatial	100 km	0.02 to 100
=)	2×10^7	~ 100%	Temporal and Spatial	250 km	0.008 to 50
±)	1×10^7	Unknown	Temporal and Spatial	100 km	poorly defined
1)	1×10^6	Unknown	Temporal and Spatial	100 km	poorly defined
-)	4×10^7	Unknown	Unknown	Not determined	2×10^{-3} to 2
+)	1×10^8	Unknown	Unknown	Not determined	Not determined
+)	1×10^8				
+)	5×10^6				
+)		Unknown	Unknown	Not determined	Not determined
+)	2×10^7	Unknown	Unknown	Not determined	Not determined
±)	6×10^7	Unknown	Unknown	Not determined	Not determined
	5×10^4	Unknown	Unknown	Not determined	Not determined
	1×10^6	Unknown	Unknown	Not determined	Not determined
		Unknown	Unknown	Not determined	Not determined
		Unknown	Unknown	Not determined	Not determined
		Unknown	Unknown	Not determined	Not determined
	1×10^7				

FOLDOUT FRAME #2

features having unknown or poorly defined characteristics, more basic experimental measurements are required before detailed determination of feasibility of their application to the cross beam experiment may be determined.

C. Atmospheric Fluctuations at High Altitudes

The density of the upper atmosphere exhibits variations which are both periodic and random in nature. In the first category are the solar cyclical variations in upper atmospheric heating rate and the diurnal, semidiurnal and lunar tides. Disturbances in density of an irregular nature also occur wherein the probability of the disturbance is correlated with solar cycle or other periodic temporal variations; magnetic storms contribute this type of density variation. The random component of atmospheric density fluctuation is primarily the result of turbulence produced by wind shear and by the decay of wave-like disturbances at high altitudes. The region of turbulence in neutral particle density extends to approximately 100 kilometers where an abrupt transition from turbulent diffusion to molecular diffusion takes place. The existence and characteristics of the "turbopause" has been the object of intense study and the source of controversy in the recent past.

Above the region known as the turbopause, atmospheric neutral density is generally in a region of high hydrodynamical stability because of the positive temperature gradient and the continued decrease in kinematic viscosity, thus making the Richardson criterian for stability tend more and more to the stable regime. The ionized gas, however, exhibits fluctuations in ion and electron density which may contribute to a fluctuating probe signal. Most of the electron density fluctuations at higher altitude are believed to be field aligned, i.e., the major axis of the density fluctuation ellipsoid is aligned along the geomagnetic field. As will be shown later in this section, little

is known about the source, length, and time scales of the fluctuations, and their mean transport characteristics such as drift rates.

Because the cross beam remote sensing technique depends upon correlation of a signal from a common volume which is statistically independent from the fluctuating signals from the remainder of the beam volume, emphasis in this section is placed upon the statistically independent sources of fluctuations, mainly the atmospheric density turbulence below the turbopause. Although it may be possible to utilize the density variations meaningfully in long wavelength disturbances such as the acoustic gravitational waves or the atmospheric tidal wave components, these are special cases which require a different analytical approach. One important exception is the study of long wavelength disturbances by their modification of emission intensity in a thin layer wherein the lower and higher altitude components of the wave will not be observed because of the lack of emission of a probe signal.

In order to evaluate the feasibility of utilizing turbulence at high altitudes as a fluctuation mechanism, knowledge of the temporal scales and length scales of these disturbances is required. Because of the lack of definitive experimental data on all aspects of this problem, an analytical interpretation of the experimental data is summarized in this section.

The parameters that are necessary to define a turbulence field are listed below:

(1) The energy $\mathcal{E}$ dissipated per unit time per unit mass by viscous action on the smallest eddies.

(2) The values of ℓ_o and ℓ_1, the scale of the smallest and largest eddies.

(3) The value W, the rate at which energy is being supplied to the largest eddies.

(4) The shape of F(k), the energy density spectral function. F(k) dk is energy per unit mass associated with eddies of wave number between k and k + dk.

(5) Expressions connecting ε, ℓ_o, ℓ_1, ν, L.

If we consider a velocity fluctuation v_1 occurring in a region of size ℓ in a fluid with kinematic viscosity ν, then it can be shown that for fluctuations of size ℓ to occur, we need the condition:

$$(v_1^3/\ell)/(v_1^2/\ell^2) = (v_1\ell/\nu) = R_e(\ell) > R_e(\text{crit})$$

$$= R_e(\ell_o)$$

where $R_e(\ell)$ is the inner Reynolds number of fluctuations of size ℓ. Experimentally v_1 has been shown to increase with ℓ, and so if ℓ_o is the scale of the smallest fluctuation, $R_e(\ell) > R_e(\ell_o)$ for all $\ell > \ell_o$. Also $t_{\ell_i} < t_{\ell_j}$ for $\ell_i < \ell_j$, then, $\ell > \ell_o$; $\ell_o \gg \ell$. Thus we have a picture of energy being handed down from larger to smaller eddies until it reaches the eddies of size ℓ_o where it is dissipated as heat by viscosity.

In discussing the atmospheric turbulence and diffusion, the important parameters are the eddy diffusion coefficient, the eddy viscosity coefficient, and the eddy coefficient of heat conduction. These coefficients are, in general, considered equal and are denoted by K. The justification for this may be found in experiments of Pasquill (Ref. 20) and with the theory of Ogura (Ref. 21).

The first estimate of ε above 80 kilometers was that of Booker (Ref. 22). Booker started with the Richardson number:

$$R_i = \frac{g}{T}\,\frac{\left(\frac{dT}{dz} + \Gamma\right)}{\left(\frac{dv}{dz}\right)^2}$$

which is considered to be a nondimensional parameter which balances the de stabilizing effects of wind shear against the stabilizing effects of gravity and thermal gradient. He also assumed the turbulence to be in a quasi equilibrium state, and, for such a state, R_i has the value of unity. The inverse function of the angular velocity of the turbulent eddy motion is the characteristic time of the largest eddies. Using a standard atmosphere, and the expressions relating ϵ, ℓ_o, ℓ_1, ν and L, various experimenters have found the values of the turbulence parameters t_o, ℓ_o, K, ν_o and ϵ, discussed above. These data are summarized in Table V.

The upper atmospheric turbulence parameters summarized in Table V may be utilized to define the applicable cross beam experimental variables, and in particular the geometrical variables which define the beam crossing characteristics. All of the data are related to altitudes below the "turbopause" at about 120 km because neutral atmospheric inhomogenieties and those present in the ionized constituents above this altitude are probably described by different theory than that utilized herein. The cross beam experimental variables appropriate to measurements of atmospheric turbulence between about 50 and 120 km are summarized in Table VI.

Two altitude ranges are defined by the particular emission feature observed. If emission of the green line (5577 A) of atomic oxygen is used as the probing signal then the altitude range over which turbulent structure may be measured is approximately 80 to 120 km. If on the other hand one of the OH Meinel bands is observed, then the altitude range accessible to experiment is approximately 50 to 90 km. Because the geometrical parameters of the cross beam system are not too sensitive to this change in the altitude range the set which is given is usable for the entire 50 to 120 km region.

However, geometrical parameters are sensitive to the scale of turbulence which is to be observed. If the main goal of the

TABLE V UPPER ATMOSPHERE TURBULENCE PARAMETER EXPERIMENTAL VALUES

t_1 (sec)	v_1 (m/sec)	l_1 (km)	t_o (sec)	v_o (m/sec)	l_o (m)	K (m^2/sec)	ε (/kg)	Altitude of Observation	Method of Observation	Experimenter
50	35	1.6	0.4	3	1.3		25	90 KM	Meteor trail expansion	Booker[22] Booker and Cohen[23]
			30	0.7	20	10^5	7×10^{-3}	"		Greenhow[24]
									Structure function of rocket N_a releases	Blamont, Teitelbaun and Barat[25]
							7×10^{-3}	"	Growth of N_a trail "globules"	Blamont and de Jaeger[26]
500	2	1	30	0.7	20	2×10^3		"		Blamont[27]
							$1.5\text{-}4 \times 10^{-2}$			Ropper & Elfard[28]
			50	1.8	90		3.2×10^{-2}	104-109		Noel[24]

TABLE VI CROSS BEAM VARIABLES FOR UPPER ATMOSPHERIC TURBULENCE MEASUREMENT

Cross Beam Variable	Upper Limit	Lower Limit	Tolerance Given by	Comments
Optical Wave Length	5577 Å	5577 Å	$\Delta\lambda$ = 3 Å determined by background rejection filters	For 80-120 km altitude range OI emission
			$\Delta\lambda$ determined by bandwidth of spectral feature	For 50-90 km altitude range OH emission
Telescope Separation, b	$2(\cot\ )h_{max}$ ≈170 km	$2(\cot\ )h_{min}$ 70 km	Position error at beam crossing altitude or altitude error at beam crossing position	
Beam Intersection Angle	60°	30°	Altitude or position error $= 2\cos^2$ for $\Delta\ \leq L/5\ \leq 6 \times 10^{-4}$ rad.	
Beam Separation Distance (, meters)	= + 2L ≥ 2km = + 2 ≥ 40m	= - 2L ≥ 2km = - 2 ≥ 40m	= L/5 or 200 m = /5 4 m	L is scale length of turbulence is micro scale length of turbulence
Beam Angular Aperture (ϕ radians)	2×10^{-3} 25×10^{-5}	4×10^{-3} 8×10^{-5}		Determined by experimental optical system design and in turn will control telescope sperture required to obtain adequate signal level.
Time Lag Increment (t, seconds)	5×10^{-2}	5×10^{-4}		Total time lag varies from 0 to $N\Delta t$ where N is the number of resolution elements in the total scan i.e. $N = 5L_i/L$
Integration Time, T_i or Integration Distance, L_i	Unknown Unknown	$T_i > L/10$ sec $L_i > L \sim 1$ km		Stationary beam system has an integration time determined by the turbulence scale L, and effective wind velocity min. A scanning system can be repeatedly swept over a region however $T_i = L_i/L$ relates these two quantities.
Scanning Speed	8 km/sec (low orbital velocity)	100 m/sec	≤ 1/5	= 100 m/sec is the typical upper atmospheric wind speed, thus a stationary beam system would experience this effective minimum scanning speed.

cross beam experiment is to define the turbulent spectrum over its entire inertial range, then the beam diameter at altitude must be approximately 1/5 of the smallest scale turbulence to be observed, i e the microscale distance ℓ_o. On the other hand, excellent information on turbulent transport in the lower wave number portion of the spectrum may be obtained with an experimental beam diameter about 1/5 of the scale length L which is typically about 1 km at an altitude of 100 km in contrast to the 20 to 100 meters microscale length. The cross beam experimental variables are given in Table VI for both cases.

D. Determination of Mean Values of Number Density from Volume Emission Rate Fluctuations

The key analytical task which is required in order to relate the measurement of a two beam correlation product to the number density profile of an atmospheric species is the complete specification of the photochemistry of the emitting species and those species with which it interacts. In this section, the general problem is outlined for different types of interactions, e.g. linear and non-linear excited state production reactions, de-excitation by collision and by radiation in the desired wavelength.

The time variation in number density of an excited species designated as N* is determined by the relative rates of two classes of processes, excitation and de-excitation. This is analytically described by the differential equation dN*/dt = Excitation rate - De-excitation rate where the excitation may be caused by radiative effects:

$$N + h\nu \longrightarrow N^*, \quad k_{er} \qquad (1)$$

by collisional effects with another species:

$$N + M \rightarrow N^* + M \text{ or } N^* + M^*, \; k_{ecm} \tag{2}$$

or by collisional effects with the same species:

$$N + N \rightarrow N^* + N \text{ or } N^* + N^*, \; k_{ecn} \tag{3}$$

The k's refer to the reaction rates with the appropriate units. Another excitational process, the Chapman reaction,[30] is important with respect to atomic oxygen and produces a cubic dependence of excitation rate upon density

$$O + O + O \rightarrow O_2^* + O^*, \quad k_{ech} \tag{4}$$

De-excitational processes which will be considered are radiative de-excitation:

$$N^* \rightarrow N + h\nu \; , \; k_{Dr} = A, \text{ the Einstein transition probability} \tag{5}$$

and collisional de-excitation with other species.

$$N^* + M \rightarrow N + M^*, \; k_{Dcm} \tag{6}$$

The differential equation representing the time behavior of the population of the excited state is:

$$dN^*/dt = k_{er} \; N + k_{ecm} \; N \, M + k_{ecn} \; N^2 + k_{ech} \; N^3 \tag{7}$$

$$- k_{Dr} \; N^* - k_{Dcm} \; N^* \, M$$

The simplest procedure to follow to solve for the volume emission rate of the radiation from process (5) in terms of the mean density

of the interacting constituents is to consider this equation to be deterministic in describing the behavior of the average population of the excited state, and to assume then that on the average a temporal steady state exists. Then the differential expression is equated to zero and solved for the volume emission intensity, $I(h\nu) = k_{Dr}\, N^*$ as a function of population of the species included in the expression:

$$I(h\nu) = \frac{k_{er}\, N + k_{ecm}\, N\, M + k_{ecn}\, N^2 + k_{ech}\, N^3}{(1 + k_{Dcm}\, M/k_{Dr})} \qquad (8)$$

In most cases, the expression can be simplified to a function of number density to a single power i.e., $I(h\nu) \propto (N)^m$, where $m = 0, 1, 2,$ or 3. In order to treat the fluctuations of volume emission intensity in terms of the number density fluctuation of the constituents, the differential form must be used:

$$\Delta I = f(N, M)\, \Delta N + g(N, M)\, \Delta M \qquad (9)$$

where

$$f(N, M) = \frac{k_{er} + k_{ecm}\, M + 2k_{ecn}\, N + 3k_{ech}\, N^2}{(1 + k_{Dcm}\, M/k_{Dr})} \qquad (10)$$

$$g(N, M) = \frac{k_{ecm}\, N}{(1 + k_{Dcm}\, M/k_{Dr})} - \frac{k_{Dcm}}{k_{Dr}}\, f(N, M)\, (1 + k_{Dcm} M/k_{Dr}) \qquad (11)$$

It is seen that there are two fluctuating components of number density which must be accounted for, the species of interest N and the average atmospheric molecule density M, which accounts for the de-excitation processes, and for the linear excitation process (equation 1). If neither of these processes are applicable to the photochemistry of the species N, then solution of the equation is greatly simplified because no ΔM terms result

Solution of this volume emission intensity fluctuation equation in terms of mean density of the species of interest, N, requires a further physical condition: the relative fluctuation ratio of all species are equal i.e., $\Delta N/N = \Delta M/M = \Delta N'/N' = \ldots$ Hence, in addition to the equivalence of the instantaneous values $\Delta N/N$ the values of the rms deviation are equivalent also, e.g $(\Delta N)^2/N^2 = (\Delta M)^2/M^2$. From a physical standpoint, this condition is justified if the fluctuation level is small enough that the second order terms in particle interactions do not seriously affect the mean density of particles. That is, the overall rates of non-linear chemical interactions are not significantly affected by departure of the density from its mean value. One must also require that the energy removed by the emitted "probe" radiation does not significantly affect the thermodynamical state of the medium with respect to the energy of the fluctuation input mechanism. In the case of upper atmospheric turbulence and airglow emission it has been shown that turbulence is not a strong energy input to the airglow process itself, hence airglow emission serves as a good non-interacting probe signal.

Insofar as the cross beam remote sensing technique operates with the correlation coefficients or the two beam product values of the fluctuating probe signal, further analysis will continue on this line. Because the measured intensity fluctuation is the integral of a large number of volume emission rates, quantities relating to local experimental volume number density must be derived from correlation measurements, not from volume emission fluctuations themselves.

The average two beam intensity fluctuation product is

$$\langle \Delta I \quad \Delta I' \rangle = f^2 \langle \Delta N^2 \rangle + g^2 \langle \Delta M^2 \rangle + 2 fg \langle \Delta M \quad \Delta N \rangle \tag{12}$$

If the value of the two beam intensity fluctuation product is obtained at two different spectral wavelengths wherein either the function f and g or both are different, i.e. $f_1 = f_2$ and/or $g_1 = g_2$, then the ratio of the two experimental values is given by:

$$T = \frac{f_1^2 \langle \Delta N^2 \rangle + g_1^2 \langle \Delta M^2 \rangle + 2 f_1 g_1 \langle \Delta N \Delta M \rangle}{f_2^2 \langle \Delta N^2 \rangle + g_2^2 \langle \Delta M^2 \rangle + 2 f_2 g_2 \langle \Delta N \Delta M \rangle} \tag{13}$$

Because the functions f_1, f_2, g_1, and g_2 are known and can be numerically evaluated as a function of altitude, the equation relating T, these functions, and the mean value of N/M may be solved through substitution of the equations $\Delta N/N = \Delta M/M$. The relationship of N/M to the experimental quantities and the functions f and g is the quadratic expression

$$\frac{N^2}{M^2} (f_1^2 - T f_2^2) + \frac{2N}{M} (f_1 g_1 - T f_2 g_2) + (g_1^2 - T g_2^2) = 0 \tag{14}$$

The complexity of this expression precludes its numerical evaluation unless a specific case is considered wherein the value of f and g are explicitly known. Therefore a specific example, that of the atomic oxygen density profile in the upper atmosphere is treated in the following section.

E Oxygen Allotrope Photochemistry

In order to show the application of oxygen airglow measurements to a current problem of research interest in aeronomy, the photochemistry of the oxygen allotropes is investigated in detail. This is probably the best known of the upper atmospheric interaction systems in terms of dependability of measured reaction rates, and agreement of the aeronomical research community as to the reactions which take place. The quantitative relationship of volume emission rates of the 5577 A OI line and the near infrared band systems of O_2 to the volume density of OI and O_2, are described.

The nighttime photochemistry of the oxygen allotropes O, O_2, O_3 in the upper atmosphere between about 60 and 120 km depends upon the excitation and loss rates of four principal excited stated, O(1D), O(1S), O_2 ($^1\Delta g$), and C_2 ($^1\Sigma_g^+$). These states are the upper levels of the transitions of the main night airglow emission for oxygen from which are emitted the 5577 A and 6300 A green and red lines of atomic oxygen, and the infrared atmospheric (IRA) and atmospheric (A) bands of molecular oxygen. Term diagrams describing these excited states with respect to ground state energy are illustrated in Figures 19 and 20. Because the intensity emitted by each of these spectral features is related to atomic oxygen density, they serve as useful remote sensing probe signals. Energetically they include virtually all of the energy emitted from oxygen in the nightglow.

The major energy source for formation of the excited states is the three body atomic oxygen recombination reaction[30] in the nighttime and the excitation of the very long-lived metastable levels ($^1\Sigma_g^+$) and ($^1\Delta_g$) of molecular oxygen in the daytime. The long radiative lifetimes of all four excited states place them in the metastable category, but the OI (1D) state is efficiently quenched by collisions in the 60-100 km region of interest, hence eliminating the 6300 A line as a usable source of probing signal from this region.

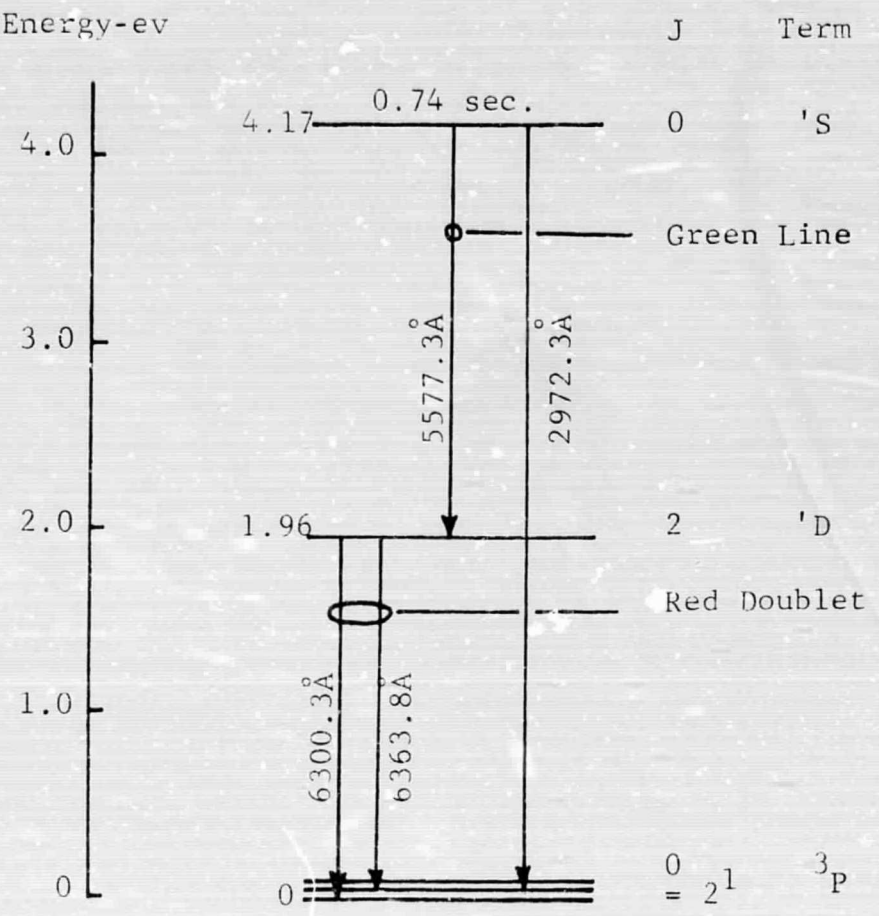


Figure 19 OI Energy Level Diagram

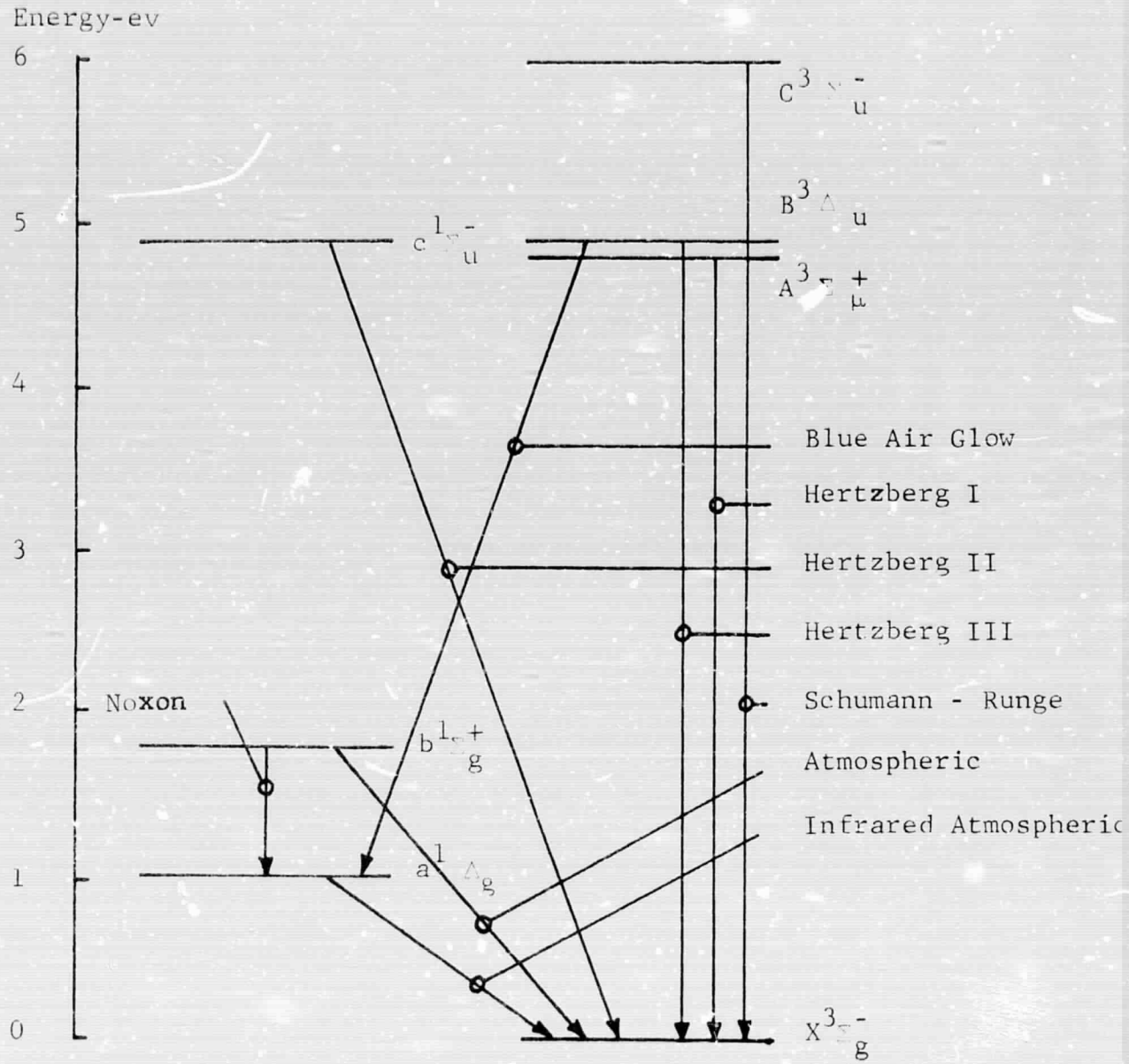


Figure 20 0_2 Energy Level Diagram

For purposes of this specific analytical inquiry, we consider the probing signals provided by the 5577 Å oxygen green line, and the 8645 Å, O_2 (0-1) atmospheric band. The volume emission intensities of these radiations are controlled by the volume densities of the excited states;

$$I_{5577\ A} = A_{5577} \quad O\ (^1D) \tag{15}$$

$$I_A = A_A \quad O_2\ (^1\Sigma_g^+) \tag{16}$$

Although the other excited state emissions are not to be considered explicitly, we must consider the effect of all of the excited states initially because their populations are coupled both through radiation processes and through collisional processes. The excited state formation and loss reactions are summarized in Table VII.

In order to construct the differential equations describing the time behavior of the excited states of interest, the importance of each reaction must be evaluated in terms of its effect upon overall state population as a function of altitude. Then, unimportant reactions may be eliminated, thus simplifying the solution of the equations. The important formation and loss reactions for the atomic oxygen states from Table VII are graphed as a function of altitude in Figures 21 to 26. Consideration of the formation and loss reactions for the O_2 ($^1\Delta_g$) state leads to the conclusion that some of the pertinent reaction rates are not well enough known to enable one to establish the most important processes. The $O_2(^1\Sigma_g^+)$ state, which is the more important of the molecular oxygen metastable levels for this analysis, is formed primarily by two processes in the nighttime and is quenched primarily through radiation of the atmospheric band. The altitude dependence of the formation rates create the possibility of further simplification of the photochemistry because below about 95 km, a single reaction

TABLE VII PRINCIPAL EXCITED STATE FORMATION AND LOSS REACTIONS (NIGHTTIME)

REACTION	RATE	REFERENCE
O(1S) EXCITATIONS		
$O + O + O \rightarrow O(1S) + O_2$	$k = 2 \times 10^{-34}$ cm^6 sec^{-1}	31
$O_2^+ + e \rightarrow O(1S) + O(3P)$	$k = 2 \times 10^{-7}$ cm^3 sec^{-1}	32
O(1S) QUENCHING REACTIONS		
$O(1S) \rightarrow O(1D) + h\nu$	$k = A_{5577} = 1.3$ sec^{-1}	33
$O(1S) + O(3P) \rightarrow 2\ O(1D)$	$k = 1 \times 10^{-13}$ cm^3 sec^{-1}	34
$O(1S) + M \rightarrow O + M^*$		
O(1D) EXCITATION REACTIONS		
$O(1S) + O(3P) \rightarrow 2O(1D)$	$k = 1 \times 10^{-13}$ cm^3 sec^{-1}	34
$O(1S) \rightarrow O(1D) + h\nu$	$k = A_{5577} = 1.3$ sec^{-1}	33
O(1D) QUENCHING REACTIONS		
$O(1D) + O_2(^3\Sigma_g^-) \rightarrow O_2(^1\Sigma_g^+) + O(3P)$	$k = 1 \times 10^{-11}$ cm^{3}sec^{-1}	35
$O(1D) + M \rightarrow O(3P) + M^*$	$k = 3 \times 10^{-11}$ cm^{3}sec^{-1}	36
$O(1D) \rightarrow O(3P) + h\nu$	$k = A_{6300} = 0.009$ sec^{-1}	33
$O_2(^1\Sigma_g^+)$ EXCITATION REACTIONS		
$O_2(^1\Delta) + O_2(^1\Delta) \rightarrow O_2(^1\Sigma_g^+) + O_2(^3\Sigma_g^-)$	$k = 3 \times 10^{-14}$ to 2×10^{-15}	37,38,39
$O(3P) + O(^3P) + M \rightarrow O_2(^1\Sigma_g^+) + M$	$k = 1.4 \times 10^{-36}$ cm^6 sec^{-1} if M=N_2	40
$O(1D) + O_2(^3\Sigma_g^-) \rightarrow O_3^* + O_2(^1\Sigma_g^+) + O(3P)$	$k = 1 \times 10^{-11}$ cm^3 sec^{-1}	41
$O_2(^1\Sigma_g^+)$ QUENCHING REACTIONS		
$O_2(^1\Sigma_g^+) \rightarrow O_2(^3\Sigma_g^-) + h\nu$ (Atmospheric)	$k = A_a = 0.14$ sec^{-1}	42,43
$O_2(^1\Sigma_g^+) \rightarrow O_2(^1\Delta_g) + h\nu$ (Noxon)	$k = A_N = 2.5 \times 10^{-3}$ sec^{-1}	44
$O_2(^1\Sigma_g^+) + M \rightarrow O_2^* + M^*$	$k = 3 \times 10^{-18}$ cm^3 sec^{-1} if M=O_2	40
	1×10^{-18} cm^3 sec^{-1} if M=N_2	44
$O_2(^1\Sigma_g^+) + O_3 \rightarrow 2O_2(^3\Sigma_g^-) + O$	$k = 4 \times 10^{-13}$ cm^2 sec^{-1}	45
$O_2(^1\Delta_g)$ EXCITATION REACTIONS		
$O(1D) + O_2 \rightarrow O_2(^1\Delta_g) + O(3P)$	$k = 1 \times 10^{-11}$ cm^3 sec^{-1}	35
$O + O + O \rightarrow O_2(^1\Delta_g) + O(1S)$	$k = 2 \times 10^{-34}$ cm^6 sec^{-1}	31
$O + O + M \rightarrow O_2(^1\Delta_g) + M$	$k = 3 \times 10^{-33}$ cm^6 sec^{-1}	46
$O_2(^1\Sigma_g^+) \rightarrow O_2(^1\Delta_g) + h\nu$ (Noxon)	$k = A_N = 2.5 \times 10^{-3}$ sec^{-1}	44
$O_2(^1\Delta_g)$ QUENCHING REACTIONS		
$O_2(^1\Delta_g) \rightarrow O_2(^3\Sigma_g^-) + h\nu$ (IRA)	$k = A_{IRA} = 1.9 \times 10^{-4}$ sec^{-1}	43
$2\ O_2(^1\Delta_g) \rightarrow O_2(^1\Sigma_g^+) + O_2(^3\Sigma_g^-)$	$k = 3 \times 10^{-14}$ cm^3 sec^{-1}	39
$O_2(^1\Delta_g) + M \rightarrow O_2(^3\Sigma_g^-) + M^*$	$k = 1 \times 10^{-18}$ cm^3 sec^{-1}	38
$O_2(^1\Delta_g) + O_3 \rightarrow 2\ O_2 + O$	$k = 1.5 \times 10^{-14}$ cm^3 sec^{-1}	47

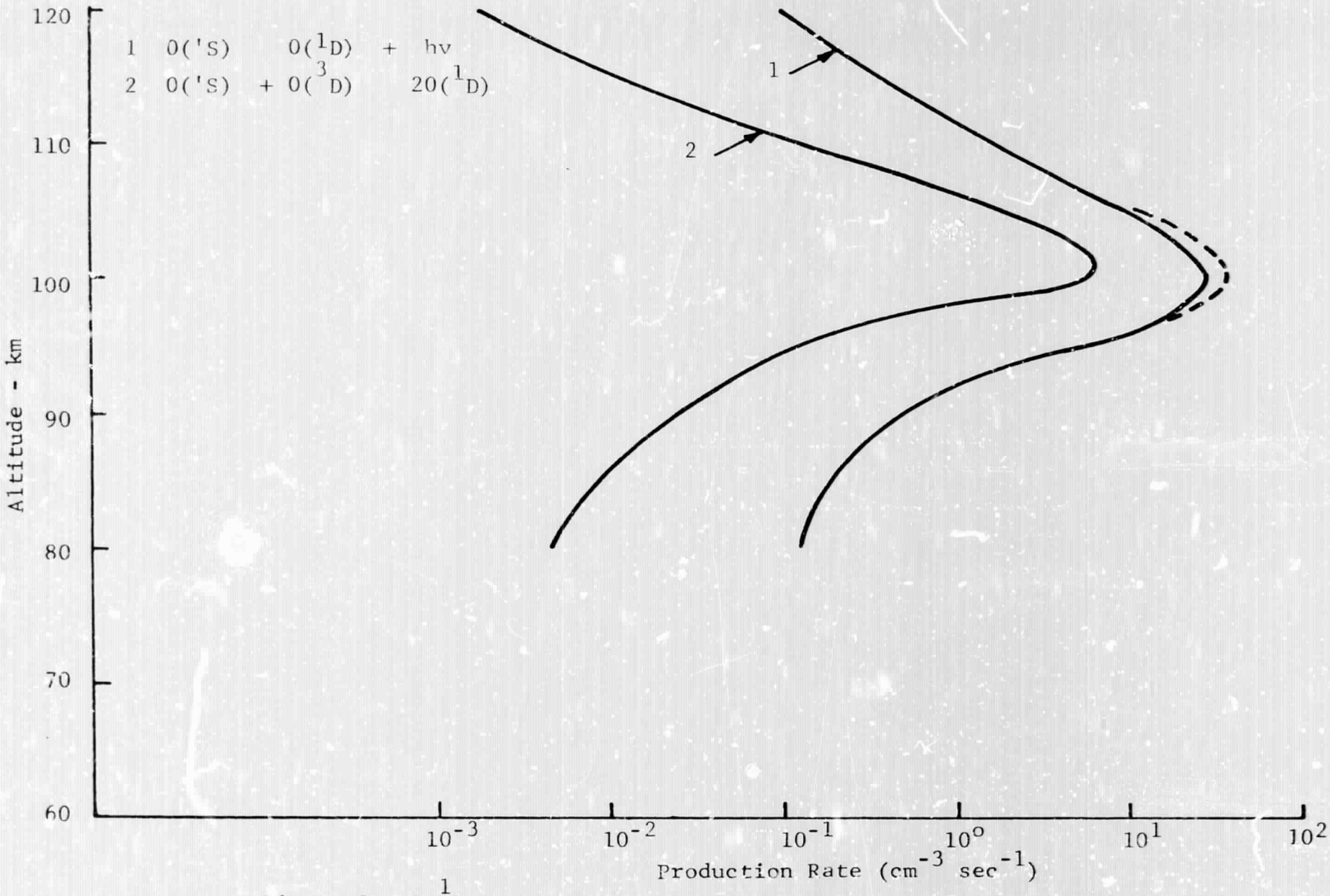


Figure 21 $O(^1D)$ Production Rates versus Altitude

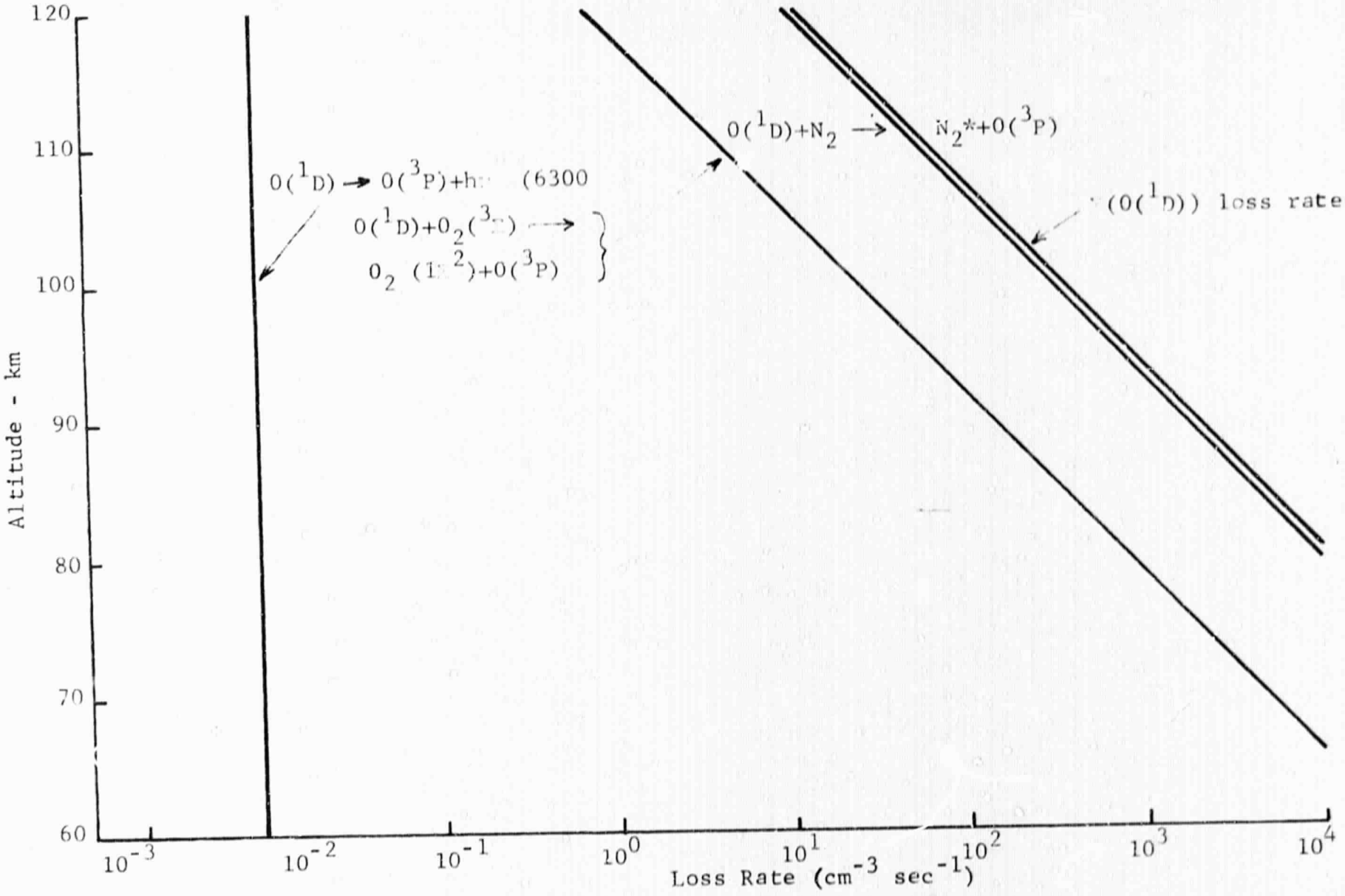


Figure 22 $O(^1D)$ Loss Rate - sec^{-1}

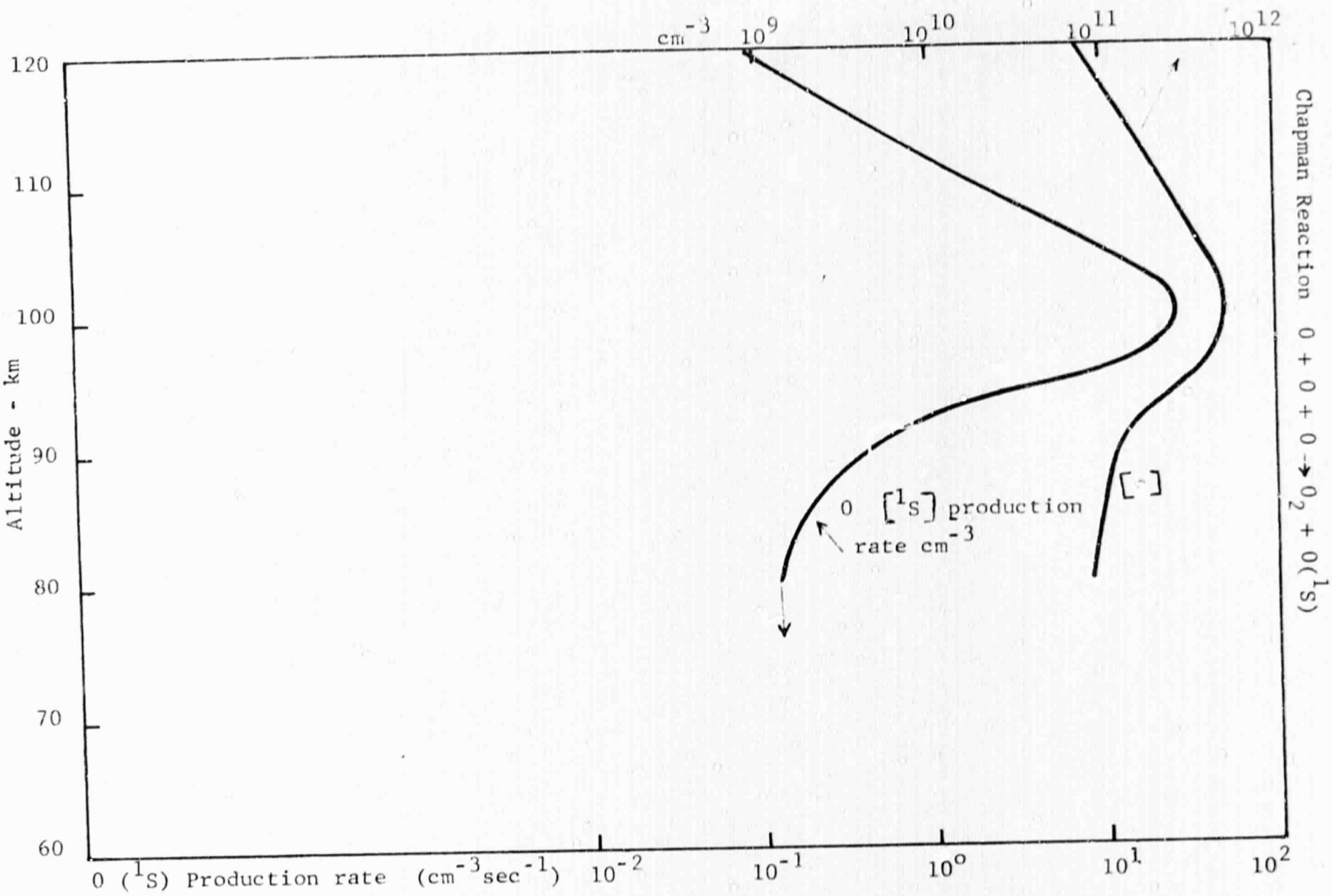


Figure 23 Atomic Oxygen Density Profile (CIRA 1965) and Chapman Reaction, $O(^1S)$ Production versus Altitude

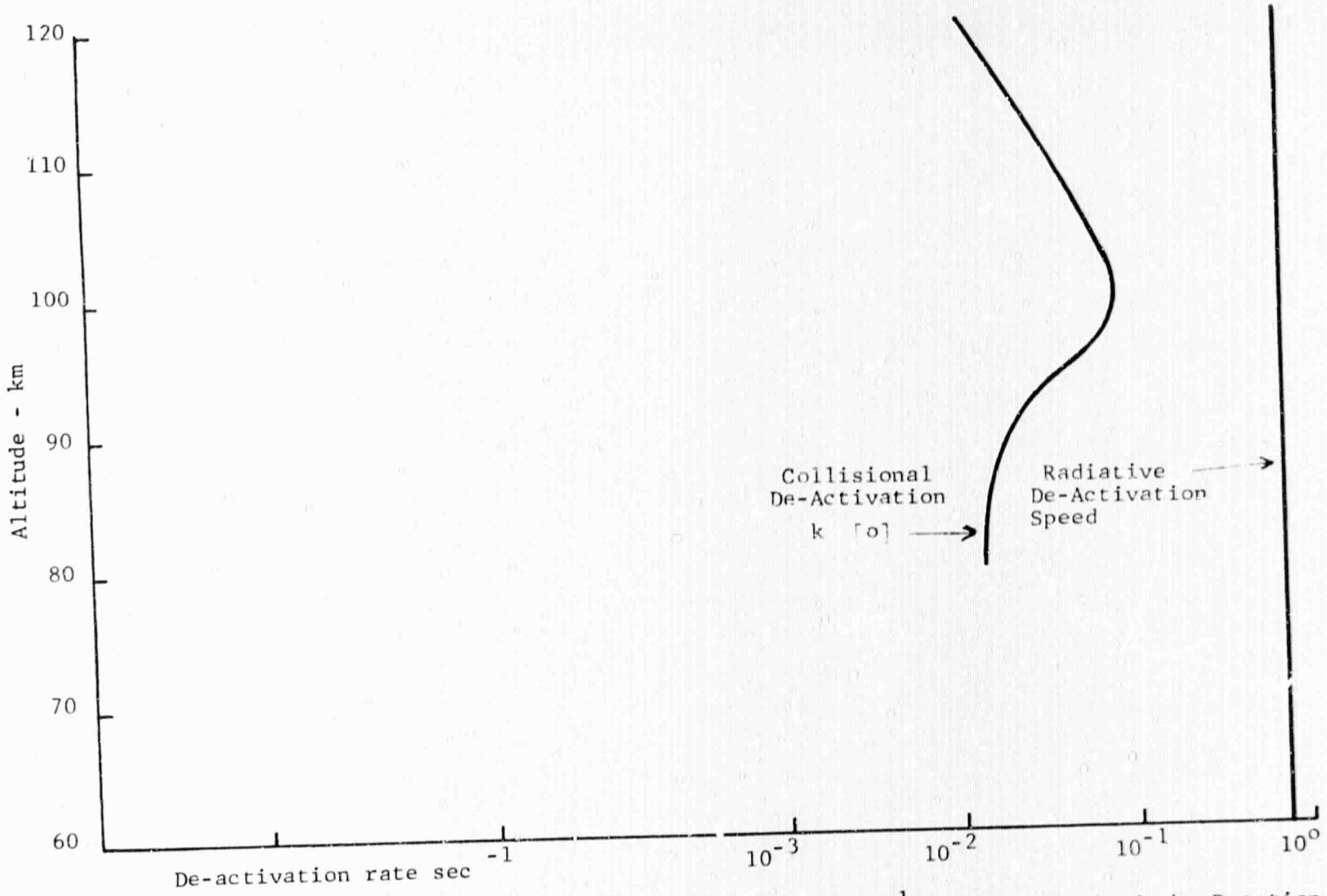


Figure 24 De-Activation Rate of Excited Oxygen Atoms (^1S) versus Altitude by Reaction

$O(^1S) + O(^3P) \quad 2O(^1D)$

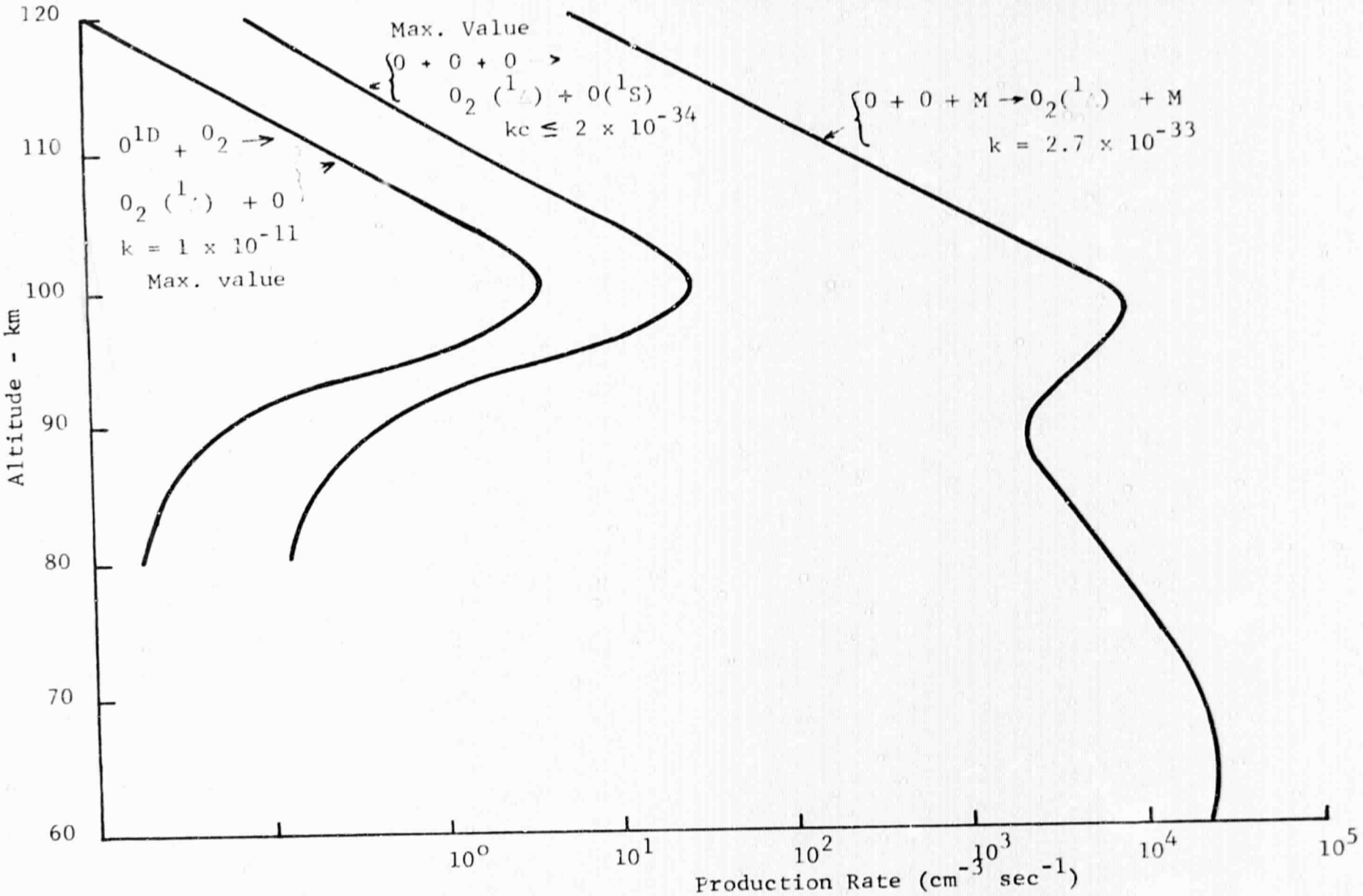


Figure 25 O_2 (1Δ) Formation Reaction

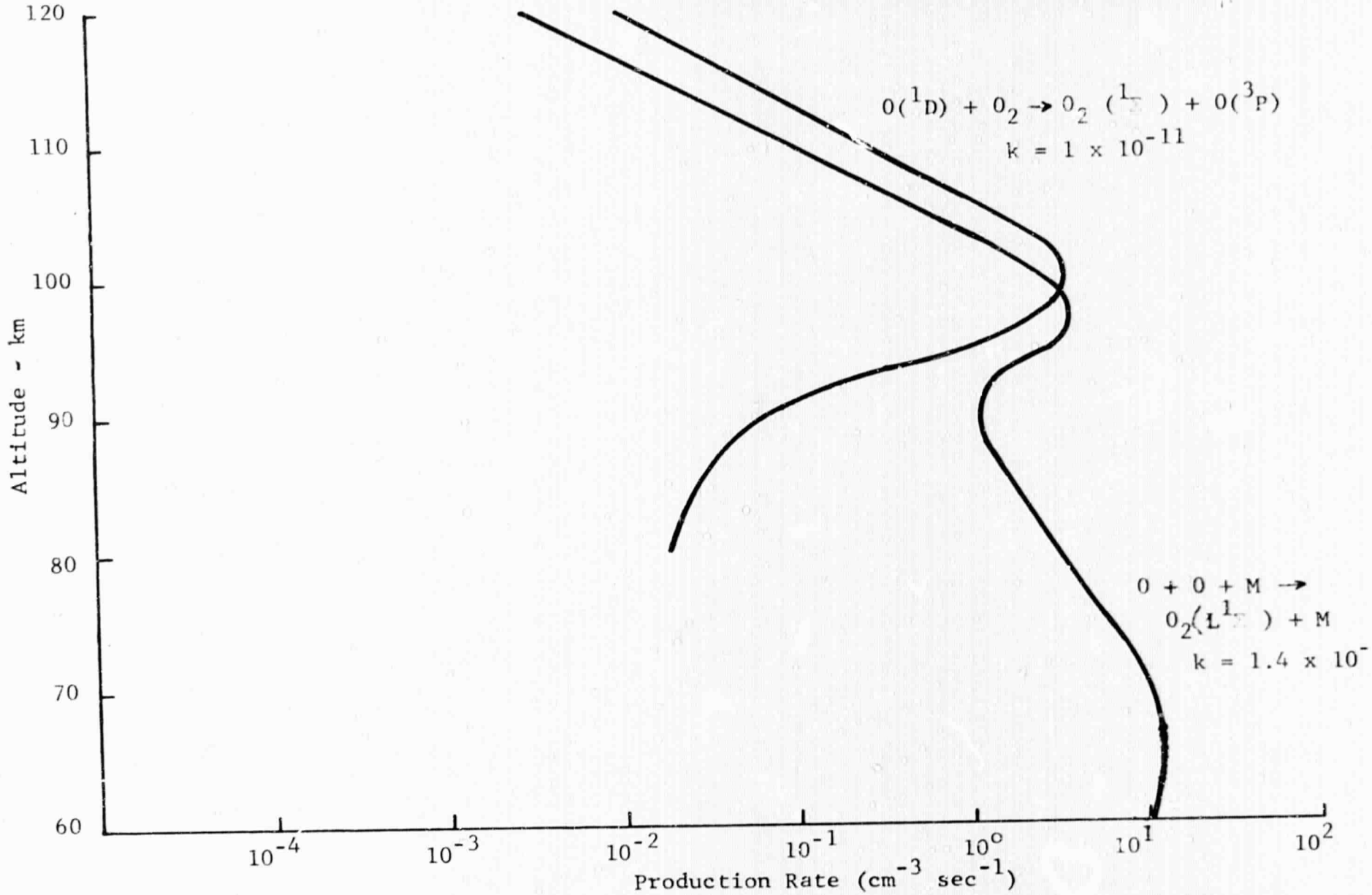


Figure 26 O_2 ($^1\Sigma$) Formation Rates versus Altitude

predominates. Above 95 km, two excitation reactions must be considered.

Explicit formulation of the differential equations for time behavior of the excited states is allowed by the previous simplification.

$$d\,O\,(^1S)/dt = k_{ech}(O)^3 - k_{Dcm}\;O(^1S) \tag{17}$$

$$d\,O_2\,(^1\Sigma_g^+)/dt = k_{ecm}\,O(^1D)\,O_2\,(^3\Sigma_g^+) + k_{ecn}(O)^2\,(M) - k_{Dr2}\;O_2\,(^1\Sigma_g^+) \tag{18}$$

The emission intensity for 5577 A and atmospheric band radiation is then:

$$I_{5577} = k_{ech}\,(O)^3 \tag{19}$$

$$I_{A8645} = k_{ecm}\,O\,(^1D)\,O_2\,(^3\Sigma_g^-) + k_{ecn}\,(O)^2\,(M) \tag{20}$$

Following the previously discussed general development, the volume emission intensity fluctuations may now be written in terms of the species density fluctuations:

$$\Delta I_{5577} = 3\,k_{ech}\,(O)^2\;\Delta(O) \tag{21}$$

$$\Delta I_{A8645} = k_{ecm}\,O\,(^1D)\;\Delta O_2\,(^3\Sigma_g^-) + k_{ecm}\,O_2(^3\Sigma_g^-)\,\Delta O(^1D) + k_{ecn}\,(O)^2\;\Delta M + 2\,k_{ecn}\,(O)\,(M)\,\Delta(O) \tag{22}$$

The altitude distribution of average volume emission rates of these features are illustrated in Figure 27.

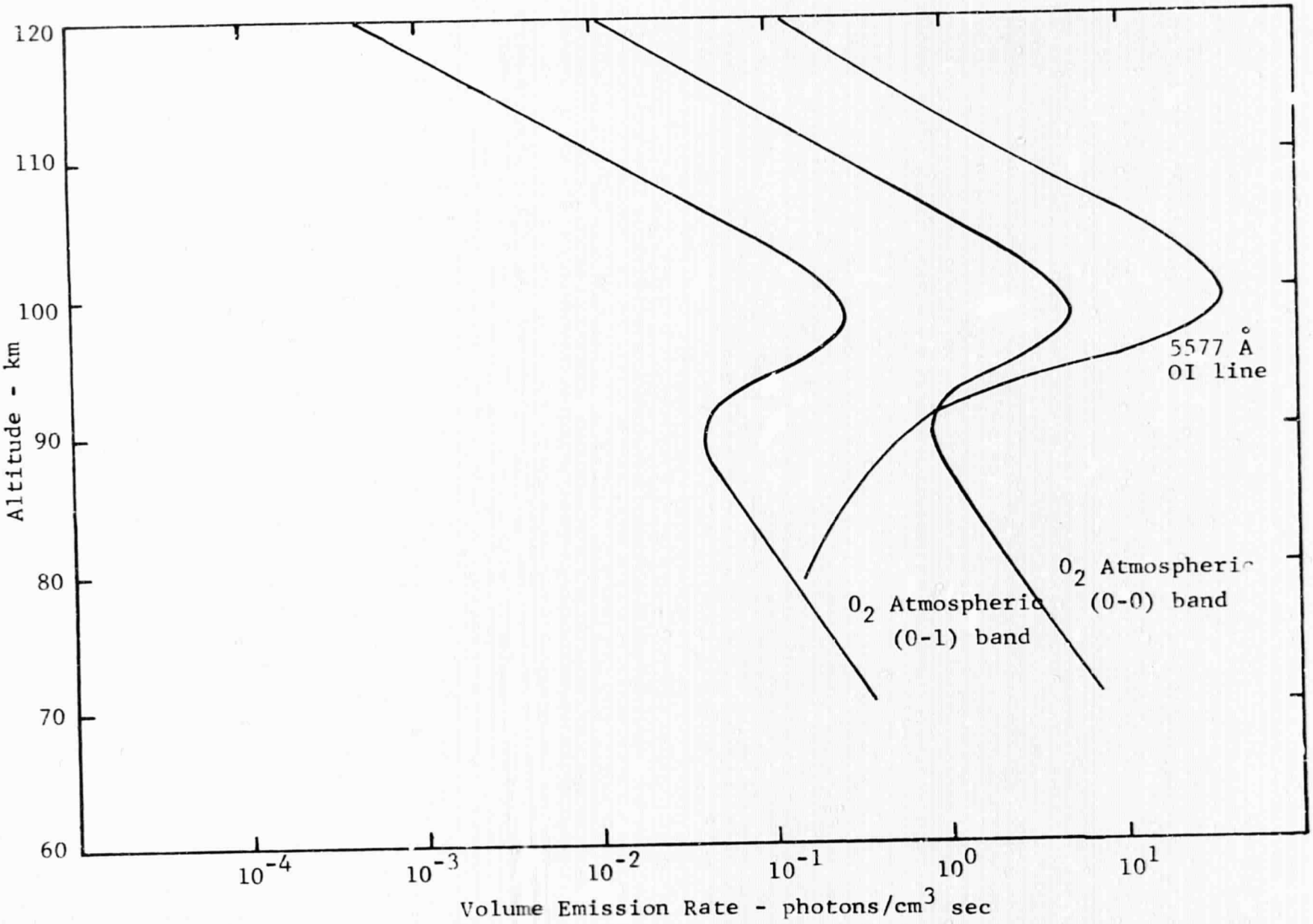


Fig. 27 Computed Volume Emission Rates versus Altitude for O_2 Atmospheric Bands and OI, 5577 Å Radiation

Below about 95 km a good approximation to the atmospheric band emission intensity fluctuation is

$$\Delta I_{A8645} = k_{ecn} (O)^2 \Delta M + 2 k_{ecn} (M) ( ) \Delta (O) \qquad (23)$$

Further analytical development is based upon two assumptions. The first, that the excited state population is approximately in steady state conditions at a constant density, allows equating the derivative to zero so solution of the equation is obtained directly in terms of the average excited state density. The second assumption is that the fractional fluctuation of species density is proportional to that of all other species i.e.,

$$\frac{\Delta O}{O} = \frac{\Delta M}{M} = \frac{\Delta N}{N} = \ldots \qquad (24)$$

This states that the fluctuations in density of individual species caused by the external mechanism which creates overall density fluctuations do not create non-linear effects with respect to other species density. That is, the fluctuations are linear about an average value for each species.

The first assumption may be justified in terms of the time required for a measurement versus the time required for a detectable change in species density. For the strongest or most non-linear reaction, the three body Chapman reaction, the maximum rate of change of atomic oxygen density is about 10^2 atoms/cm^3 second. This is compared with an average density of 10^{12} atoms/cm^3. It is obvious that even very long integration times (10^4 seconds) will not produce significant changes in average density. The emission from the excited states is closely coupled to average density and its changes because the excited states lifetimes for O(1D) and O_2 ($^1\Sigma_g^+$) are about 0.7 and 7 seconds, respectively. Fluctuations in density faster than this value will be integrated out if strictly temporal averaging is considered. (Note: if spatial averaging is accomplished by sweeping one or both beams, then this

argument is unnecessary).

The second assumption is based upon the physical mechanism which drives the fluctuations. It is reasonable to assume that on a small scale, the overall density fluctuation acts upon each species in the same manner. The constancy of the fractional fluctuation ratio with altitude is not required, however, nor does this assumption have to hold for times longer than a single measurement. This additionally implies that a fluctuating density does not drive the system away from equilibrium through a strong non-linear interaction such as the Chapman three body recombination of atomic oxygen. This assumption may be quantitatively evaluated by consideration of the expansion of the equation for the number density of the excited O(1S) state:

$$\Delta I_{5577} = I_{5577} - \bar{I}_{5577} = k_{ech} (O^3 - \bar{O}^3) \qquad (25)$$

The instantaneous value of atomic oxygen density is $O = \bar{O} + \Delta O$, thus

$$\Delta I_{5577} = k_{ech} (\bar{O}^3 + 3\bar{O}^2 \Delta O + 3 \bar{O} \Delta O^2 + (\Delta O)^3 - \bar{O}^3) \qquad (26)$$

The ratio of the first fluctuation term, $O^2 (\Delta O)$, to the second, $O(\Delta O)^2$, is simply proportional to the inverse of the fractional fluctuation level. For example if the fractional fluctuation is 1%, then the ratio of the first fluctuation term to the second is 100, and the error introduced by ignoring the second term is about 1% on the measured value of the first or linear term. For smaller fractional fluctuation values, even smaller errors result from this assumption. For larger fractional fluctuation values, for example, as could exist in a spatial sweep of the 5577 A line, errors would soon approach the 100 percent value. However, even this large an error could conceivably be acceptable because the density of atomic oxygen at a given altitude may not be known to better than an order of magnitude.

Using the values of the excitation and quenching reaction rates for the states of interest, it is possible to construct a quantitative evaluation of the theory and to derive the variation of magnitude of the fluctuation ratio with altitude expressed in Equation 13. The theory in this section allows explicit evaluation of the functions f_1, g_1, f_2 of the previous section. These are:

$$f_1 = 3\, k_{ech}\, (O)^2$$

$$g_1 = 0$$

$$f_2 = k_{ecm}\left[(O\ {}^1D)\ \frac{(O_2\ {}^1\Sigma_g^+)}{(O)} + \frac{(O_2\ {}^3\Sigma_g^-)\ (O\ {}^1D)}{(O)}\right] + 3\, k_{ecn}(O)(M)$$

$$g_2 = 0$$

Then

$$T = \left[3\, k_{ech}\, (O)^2\right]^2 \Big/ \left\{k_{ecm}\left[\frac{(O\ {}^1D)\ (O_2\ {}^1\Sigma_g^+)}{(O)} + \frac{(O_2\ {}^3\Sigma_g^-)\ (O\ {}^1D)}{(O)}\right] + 3\, k_{ecn}\, (O)\ (M)\right\}^2$$

These expressions were obtained through use of the relationship $\Delta O/\bar{O} = \Delta M/\bar{M} = \Delta O_2/\bar{O}_2$ etc. Because the several fluctuating quantities may be related to either the atomic oxygen density fluctuation or to the neutral density fluctuation in more than one way, the functions f and g are not unique. Depending upon the particular theory and application, these functions may be chosen to allow the simplest numerical computations to be done. It may be seen that the experimental value of T thus depends upon only one unknown, the atomic oxygen average density, the analytically determined mean densities of the excited states

$O(^1D)$ and $O_2(\Sigma_g^+)$, and the mean value of neutral particle density M which may be determined from a model atmosphere with sufficient accuracy. The fluctuating quantities $\langle \Delta O \rangle^2$ are eliminated. In practice, insofar as the mean values of the excited state densities would not be directly measurable, their computed values would most likely be varied in order to obtain a best fit to the experimental data.

III. SUMMARY AND CONCLUSIONS

The feasibility study reported herein has investigated the applications of the cross beam remote sensing technique to problems of atmospheric research. Two general classes of problems have been considered, those related to the troposphere and to meteorology, and those related to upper atmospheric aeronomy. The latter class has received primary attention in this study.

The results may be summarized simply as follows:

1) The technological feasibility of measuring fluctuations in intensity of scattered sunlight from the troposphere as a remote sensing probe was demonstrated analytically.

2) The technological feasibility of measuring fluctuations in intensity of non-thermal radiation emitted from the upper atmosphere as a remote sensing probe signal was demonstrated analytically.

3) Feasibility of interpreting the intensity fluctuations from upper atmosphere non-thermal emission from oxygen allotropes in terms of the mean density profile of atomic oxygen was demonstrated analytically.

In conclusion, it must be emphasized that feasibility of application of the cross beam remote sensing experiment must be measured against the specific application and must include consideration of the elements which constitute feasibility. In the limiting sense of this statement, the study reported herein is very restricted in that the methodology of proof of feasibility is outlined and applied in detail to only a limited class of problems.

REFERENCES

1. St. John, A. D., W. D. Glauz,"Study of Atmospheric and AAP Objectives of Cross Beam Experiments", NASA Contractor Report CR 61191, Feb. 1968.
2. Montgomery, A. J., Space Science Reviews, in publication.
3. Stephens, J. B., V. A. Sandborn, and A. J. Montgomery, "Remote Wind Detection with the Cross Beam Method at Tower Heights", in Aero Astrodynamics Research Review No. 7. NASA TM-X 53782, October 15, 1968.
4. Fisher, M. J., and F. R. Krause, J. Fluid Mech. 28, 705, 1967.
5. Davies, W. O., and R. W. Deuel, "Atmospheric Applications of the Cross Beam Technique", in Aero Astrodynamics Research Review No. 5, NASA TM-X 53568, October 15, 1966.
6. Sears, R. D., Feasible Methods of Simulating Nuclear Interference", Final Report on Contract DA 49-146-XZ-090, 1962.
7. Wolff, M., Trans. Amer. Geophys. Union 47, 75, 1966.
8. Krause, F. R., S. S. Hu, and A. J. Montgomery, "On Cross Beam Monitoring of Atmospheric Winds and Turbulence with Two Orbiting Telescopes", NASA TM-X 53538, Nov. 14, 1966.
9. Krause, F. R., A. J. Montgomery, W. O. Davies, and M. J. Fisher, "Optical Methods for Remote Sensing of Local Thermodynamic Properties and Turbulence", Aero Astrodynamics Research Review No. 5, NASA TM-X 53568, Oct. 15, 1966.
10. Krause, F. R., J. C. LaFrance, S. V. Paranjape, and J. B. Stephens, "Feasibility and Potential of Atmospheric Crossed Beam Experiments", Aero Astrodynamics Research Review No. 5, NASA TM-X 53568, Oct. 15, 1966.
11. Davies, W. O., "Study of Noise Generation and Turbulent Fluxes on Saturn 1B and V Exhausts", Final Report on Contract NAS8-20108, Part II, May 1967.
12. Valley, S. L., ed., "Handbook of Geophysics and Space

REFERENCES - Cont'd

Environments," P7-3, McGraw Hill Book Co., New York 1965.

13. Sears, R. D., Monthly Report No. 4 on Contract NAS8-20107 Mod. 3, Nov. 1966.

14. Coulson, K. L., J. V. Dave, and Z. Sekera, "Tables Related to Radiation Emerging from a Planetary Atmosphere with Rayleigh Scattering" University of California Press, Berkeley, 1960.

15. Hughes, J. V., Applied Optics, 3, 1135, 1964.

16. Project Mesa, "Present and Future Air Force Needs for Environmental Measurements", Geophysics Corp. of America, January 1962.

17. Sloan, R., J. H. Shaw, and D. Williams, J. Opt. Soc. Am. 45, 2455, 1955.

18. Friedman, H., in Physics of the Upper Atmosphere" edited by J. R. Ratcliffe Academic Press, New York, 1960, p. 197.

19. Broadfoot, A. L., and K. R. Kendall, J. Geophys. Res. 73, 426, 1968.

20. Pasquill, F., Proc. Roy. Soc. A198, 116, 1949.

21. Ogura, Y., Advances in Geophys. 6, 175, 1959.

22. Booker, H. G., J. Geophys. Res. 61, 670, 1956.

23. Booker, H. G. and R. Cohen, J. Geophys. Res. 61, 707, 1956.

24. Greenhow, J. S., J. Geophys. Res. 64, 2208, 1959.

25. Blamont, J. E., H. Teitelbaum, and J. Barat, Ann. Geophys. 24, 115, 1968.

26. Blamont, J. E., and C. de Jaeger, Ann. Geophys. 17, 134, 1961.

27. Blamont, J. E., Planet. and Space Sci. 10, 89, 1962.

28. Ropper, R. G. and W. G. Elford, Nature 197, 963, 1963.

29. Noel, T. M., J. Geophys. Res. 68, 2862, 1963.

30. Chapman, S., Proc. Phys. Soc. (London) 43, 26, 1931.

31. Young, R. A. and G. Black, J. Chem. Phys. 44, 3741(1966).

32. Biondi, M. A., Ann. Geophys. 20, 34, 1964.

REFERENCES - Cont'd

33. Garstang, R. H., Monthly Not. Roy. Astron. Soc. 111, 115, 1951.
34. Bates, D. R., Disc. Faraday Soc. 37, 21, 1964.
35. Seaton, Astrophys. J. 127, 54, 1958.
36. Snelling, D. R., and E. J. Bair, J. Chem. Phys. 47, 228 (1967).
37. Wayne, R. P., Photochem. and Photobiol. 5, 889, 1966.
38. Winer, A. M., and K. D. Bayes, J. Phys. Chem. 70, 302, 1966.
39. Young, R. A., and G. Black, J. Chem. Phys. 42, 3740, 1965.
40. Young, R. A. and R. L. Sharpless, J. Geophys. Res. 67, 3871, 1962.
41. Young, R. A., and G. Black, J. Chem. Phys. 47, 2311, 1967.
42. Noxon, J., Can. J. Phys. 39, 1110, 1961.
43. Nicholls, R. W., Ann. Geophys. 20, 144, 1964.
44. Wayne, R. P., Quart. J. Roy. Met. Soc. 93, 69, 1967.
45. March, R. E., S. G. Furnival, and H. I. Schiff, Photochem and Photobiol. 4, 971, 1965, and Disc. Faraday Soc. 37, 38, 1965.
46. Reeves, R. R., G. Manella, and P. Haerteck, J. Chem. Phys. 32, 632, 1960.
47. Mathias, A. and H. I. Schiff, Disc. Faraday Soc. 37, 38, 1961.